WL-TR-93-4013

# CONTINUOUS FABRICATION OF SiC FIBER TOWS BY CHEMICAL VAPOR DEPOSITION


W.J. Lackey, J.A. Hanigofsky, G.B. Freeman,
R.D. Hardin,B.N. Beckloff, D.M. Emmerich,
A. Prasad, M.D. Ellenburg, J. Pugh,
M.D. Langman, and J.S. Lewis

MATERIALS SCIENCE AND TECHNOLOGY LABORATORY
GEORGIA TECH RESEARCH INSTITUTE
ATLANTA, GEORGIA 30332

JANUARY 1993

FINAL REPORT FOR SEPT. 1991 - DEC. 1992

APPROVED FOR PUBLIC RELEASE;
DISTRIBUTION IS UNLIMITED



MATERIALS DIRECTORATE
WRIGHT LABORATORY
AIR FORCE MATERIEL COMMAND
WRIGHT PATTERSON AFB, OHIO 45433-7734



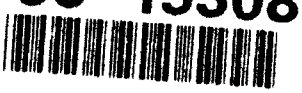

## NOTICE

When Government drawings, specifications, or other data are used for any purpose other than in connection with a definitely Government-related procurement, the United States Government incurs no responsibility or any obligation whatsoever. The fact that the government may have formulated or in any way supplied the said drawings, specifications, or other data, is not to be regarded by implication or otherwise in any manner construed, as licensing the holder, or any other person or corporation; or as conveying any rights or permission to manufacture, use, or sell any patented invention that may in any way be related thereto.

This report is releasable to the National Technical Information Service (NTIS). At NTIS, it will be available to the general public, including foreign nations.

This technical report has been reviewed and is approved for publication.

PAUL D. JERO, Project Engineer
Materials Development Branch
Metals and Ceramics Division

WALTER H. REIMANN, Chief
Materials Development Branch
Metals and Ceramics Division

NORMAN M. GEYER, Acting Deputy Director
Metals and Ceramics Division

If your address has changed, if you wish to be removed from our mailing list, or if the addressee is no longer employed by your organization please notify WL/MLLM, WPAFB, OH 45433-6533 to help us maintain a current mailing list.

Copies of this report should not be returned unless return is required by security considerations, contractual obligations, or notice on a specific document.

# REPORT DOCUMENTATION PAGE

Form Approved
OMB No 0704 0188



| 1. AGENCY USE ONLY (Leave blank) | 2. REPORT DATE | 3. REPORT TYPE AND DATES COVERED |
|---|---|---|
| | 1 January 1993 | Final, 9/1/91 - 12/31/92 |

**4. TITLE AND SUBTITLE**

Continuous Fabrication of SiC Fiber Tows by Chemical Vapor Deposition

**5. FUNDING NUMBERS**

PE 62102F
PR 2420
TA 01
WU 99

**6. AUTHOR(S)**

W. J. Lackey, J. A. Hanigofsky, G. B. Freeman
R. D. Hardin, B. N. Beckloff, D. M. Emmerich, A. Prasad,
M. D. Ellenburg, J. Pugh, M. D. Langman, and J. S. Lewis

**7. PERFORMING ORGANIZATION NAME(S) AND ADDRESS(ES)**

Materials Science and Technology Laboratory
Georgia Tech Research Institute
Georgia Institute of Technology
Atlanta, Georgia 30332

**8. PERFORMING ORGANIZATION REPORT NUMBER**

A-9056

**9. SPONSORING/MONITORING AGENCY NAME(S) AND ADDRESS(ES)**

Materials Directorate (WL/MLLM)
Wright Laboratory
Air Force Materiel Command
Wright Patterson AFB, OH 45433-7734
WL/MLLM Attn: Jero 513-255-9818

**10. SPONSORING/MONITORING AGENCY REPORT NUMBER**

WL-TR-93-4013

**11. SUPPLEMENTARY NOTES**

**12a. DISTRIBUTION/AVAILABILITY STATEMENT**

Approved for public release; distribution is unlimited.

**12b. DISTRIBUTION CODE**

**13. ABSTRACT** (Maximum 200 words)

The objective of this 15-month effort was to determine the feasibility of preparing small diameter SiC fiber tows by chemical vapor deposition for use as reinforcing fibers in ceramic and metal matrix composites. The proposed goal of codepositing SiC + $Si_3N_4$ was modified 2 months into the project in order to concentrate on fiber coating technology for SiC fiber development only. Our approach was to develop spreading techniques for filaments of the substrate tow so that SiC could be rapidly deposited without bonding the filaments together. Following some initial experiments, a statistical processing study was completed to define processing conditions where the desired 5 μm SiC coating thickness would be achieved. Processing-property correlations were determined using multiple regression analysis. Stress calculations were used to aide in substrate selection--the carbon fiber which had the minimal fiber/coating stress due to thermal expansion mismatch was determined to be the Amoco T-300, unsized and untwisted fiber. Several fiber spreading techniques were evaluated to minimize fiber agglomeration. Cyclic tension, in conjunction with gas jets or stationary and moving rollers was determined to be ineffective for spreading the fiber tow. The most promising results, however, were obtained from electromagnetic spreading of the fiber tow.

| 14. SUBJECT TERMS | 15. NUMBER OF PAGES |
|---|---|
| Fibers, Silicon Carbide, Chemical Vapor Deposition | 98 |
| | 16. PRICE CODE |

| 17. SECURITY CLASSIFICATION OF REPORT | 18. SECURITY CLASSIFICATION OF THIS PAGE | 19. SECURITY CLASSIFICATION OF ABSTRACT | 20. LIMITATION OF ABSTRACT |
|---|---|---|---|
| Unclassified | Unclassified | Unclassified | UL |

TABLE OF CONTENTS

## TABLE OF CONTENTS
(continued)

## LIST OF FIGURES

LIST OF FIGURES
(continued)

## LIST OF TABLES

# CONTINUOUS FABRICATION OF SIC FIBER TOWS BY CHEMICAL VAPOR DEPOSITION

## 1. EXECUTIVE SUMMARY

The objective of this 15 month effort was to determine the feasibility of preparing small diameter SiC fiber tows by chemical vapor deposition (CVD) for use as reinforcing fibers in ceramic and metal matrix composites. The proposed goal of codepositing SiC + $Si_3N_4$ was modified 2 months into the project in order to concentrate on fiber coating technology for SiC fiber development only. Our approach was to develop spreading techniques for filaments of the substrate tow so that SiC could be rapidly deposited without bonding the filaments together. Following some initial experiments, a statistical processing study was completed to define processing conditions where the desired 5 $\mu$m SiC coating thickness would be achieved. Processing-property correlations were determined using multiple regression analysis. Stress calculations were used to aide in substrate selection--the carbon fiber which had the minimal fiber/coating stress due to thermal expansion mismatch was determined to be the Amoco T-300, unsized and untwisted fiber.

Several fiber spreading techniques were evaluated to minimize fiber agglomeration. Cyclic tension, in conjunction with gas jets or stationary and moving rollers, was determined to be ineffective for spreading the fiber tow. Fiber tow splitting also did not consistently spread the filaments apart during coating. Pneumatic spreading of the tow resulted in spread fibers with minimal agglomeration. The most promising results, however, were obtained from

electromagnetic spreading of the fiber tow. This technique was investigated in a cold walled system, and resulted in extensive spreading (factor of 10) of the fiber tow. Spreading at 1 atm was also accomplished, which could lead to a more economical process due to faster coating rates achievable at higher pressures.

Two literature publications have resulted from this work; several conference presentations were also delivered as part of this project. Part of one doctoral thesis in Materials Engineering and one master's thesis have resulted from this work.

## 2. INTRODUCTION

Advanced ceramic fibers are needed for use as reinforcement for ceramic and metal matrix composites. Such composite materials are receiving increased attention for both aerospace and industrial applications. The fiber reinforcement enhances toughness, strength, stiffness, and creep resistance for both ceramic and metal matrix composites. In many instances high temperatures are involved in the fabrication process and/or the in-service environment. Often the desired temperature exceeds the fiber capability, i.e., the fiber strength degrades significantly in just a few hours. For example Nicalon, Tyranno, and Nextel (8-20 $\mu$m diameter filaments), which are three of the more popular fiber tows, degrade at temperatures above $\sim$1200°C. Textron and Sigma's SiC monofilament ($\sim$100-150 $\mu$m diameter) can survive to $\sim$1400°C and are useful in several ceramic and metal matrix composites but their large size keeps them from being an optimal reinforcement of ceramics; the large size complicates fabrication of thin components and the desired increase in toughness is not always achieved with a large fiber. In some instances a large diameter fiber appears to act as a flaw of size similar to that of the fiber. The large monofilaments are also not sufficiently flexible; weaving and the fabrication of samples with small radii of curvature are not as easy as with small "textile grade" fibers. Also, the economics of monofilament production are poor. The higher surface area of a tow, compared to a monofilament, and the reduced thickness of coating which must be deposited favor, at least for a CVD process, the production of tows. SiC has the desired attributes of light weight, stiffness, strength, and chemical compatibility with desired matrices such as SiC, $Si_3N_4$, and $Al_2O_3$. To our knowledge, no one, with the possible exception of a

small effort at SUNY-Buffalo, is pursuing small diameter SiC fiber multifilament tows via CVD processing.

The goal of this project was to demonstrate the feasibility of fabricating strong, thermally stable, continuous SiC fiber tows by the CVD of SiC onto commercially available carbon or oxide fiber tows. As shown schematically in Figure 1, deposition of a coating which has a thickness of 5 $\mu$m onto a 5 $\mu$m diameter fiber substrate yields a fiber which is 89 vol % SiC. An existing continuous fiber coating system was used and the extensive background on fiber coating, in general, and the CVD of SiC, in particular, provide an excellent technology base to support the project.

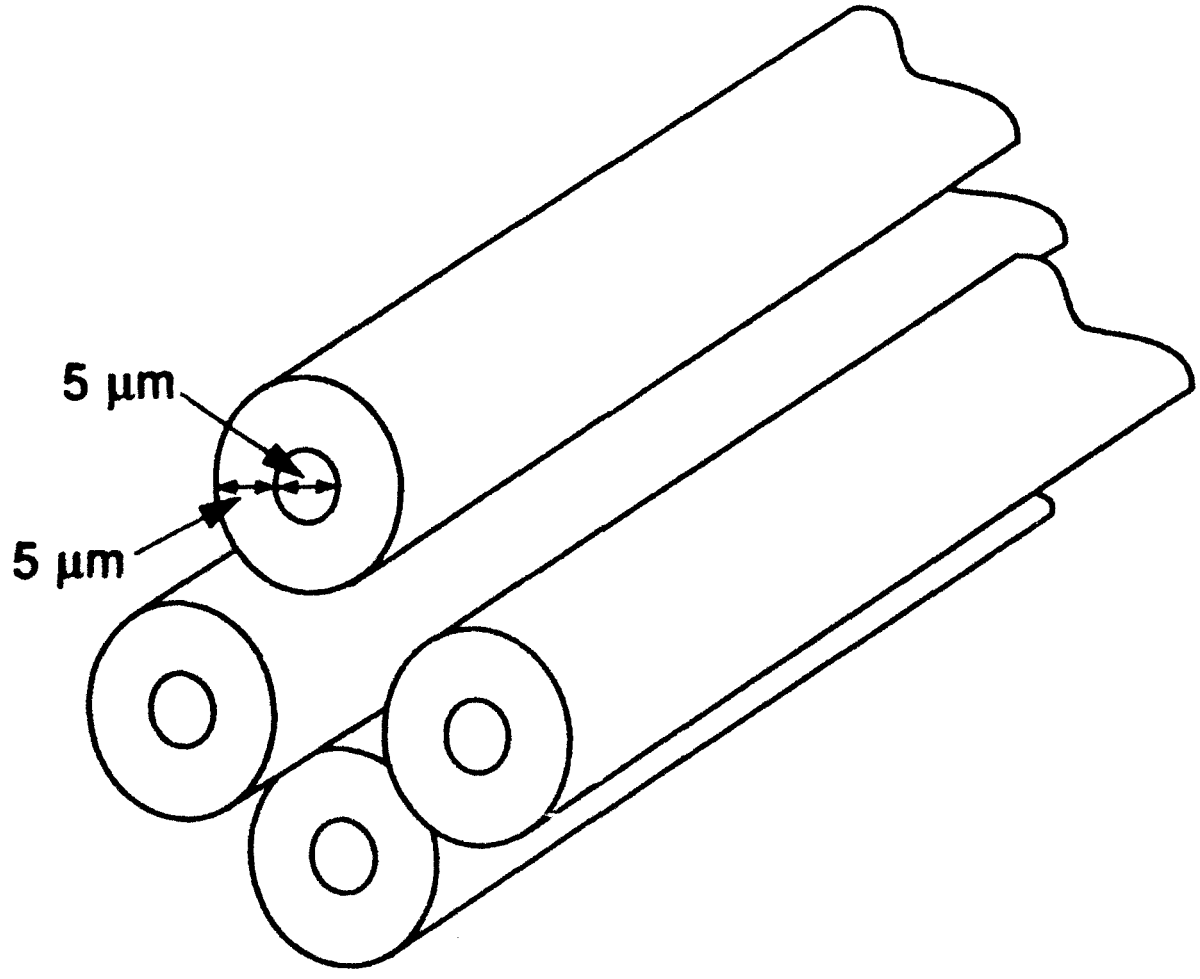


Figure 1. Schematic of the SiC fiber tow deposited by chemical vapor deposition on a carbon fiber tow substrate.

## 3. BACKGROUND

### 3-1. Fiber Coating Literature Review

In order for fibers to properly fulfill their role as reinforcements in ceramic and metal matrix composites and carbon-carbon, it is often necessary to coat the fiber with some other material. The function of the coating may be to protect the fiber during subsequent processing or in-service use, to provide compatibility with the matrix, or to provide the desired degree of bonding between the fiber and matrix in order to optimize toughness, strength, creep, and other properties. Such coatings are often less than 1 $\mu$m thick and are frequently about 0.1 $\mu$m thick. By applying considerably more coating it is possible to prepare CVD monofilaments or tows where a smaller fiber serves as the substrate.

There has been extensive prior use of CVD for coating of fibers, felt, tape, and cloth and the process is increasingly being recognized as having commercial appeal.[1-39] Some of the advantages of CVD are (1) high deposition rate, (2) high purity, (3) applicability to oxides, carbides, nitrides, borides, silicides, or metals, and (4) the deposits are usually crystalline and thermally stable. A further advantage compared to line of sight processes, is that fiber tows can be infiltrated, i.e., each filament is uniformly coated. Fibers fabricated by a CVD process are typically dense, fine grained, and possess high strength.

Much of the prior work has relied on batch processing but extensive progress has been made in developing continuous fiber coating equipment and processes. Notable prior work is that at Los Alamos National Laboratory,[14,18] the University of Karlsruhe,[6,9,11,20,26,34] and Textron's commercial use of a continuous CVD process to make B and SiC monofilaments.[7,16,21,31]

Continuous fiber coating equipment and processes have been recently reviewed by Lackey et al.[39] The fiber may be heated by one of several means. These include (1) electrical heating of the fiber alone by passing a current through it, (2) lasers, (3) induction, (4) microwaves, (5) infrared lamps, and (6) the resistive hot wall method. Plasma assisted CVD is also possible but it has the disadvantage that the deposition rates are usually low. Some of the techniques permit operation with a cold wall which has the advantages of reducing reagent consumption and depletion and minimizing constriction of the reaction chamber as a result of excessive coating deposition on the walls of the chamber. Many of these methods have the disadvantage that they are restricted to use with fibers which are electrically conducting. The resistively heated, hot wall system has the advantages of simplicity, reliability, and applicability to both conducting and insulating fibers. This method avoids the need for mercury seals and contacts which have the disadvantages of (1) possibly contaminating the coating and (2) being difficult to operate at reduced pressure. A schematic of the Georgia Tech continuous fiber coating system is shown in Figure 2. This hot walled system consists of a CVD furnace with two spool enclosures at the top and bottom which allow for visual fiber monitoring during the process and also allows for both atmospheric and vacuum processing.

An optimal continuous fiber coating system should provide control over the speed at which the fiber is pulled through the furnace. The desired speed varies over a large range depending primarily on the material being deposited, the length of the coating zone, and the desired coating thickness. Literature values for fiber pull speed vary from 0.2 to 100 inches per minute. Many CVD coatings are capable of being deposited at rates equal to or greater than several microns per minute. Thus, for a coating zone only 1 foot in length, a fiber pull speed

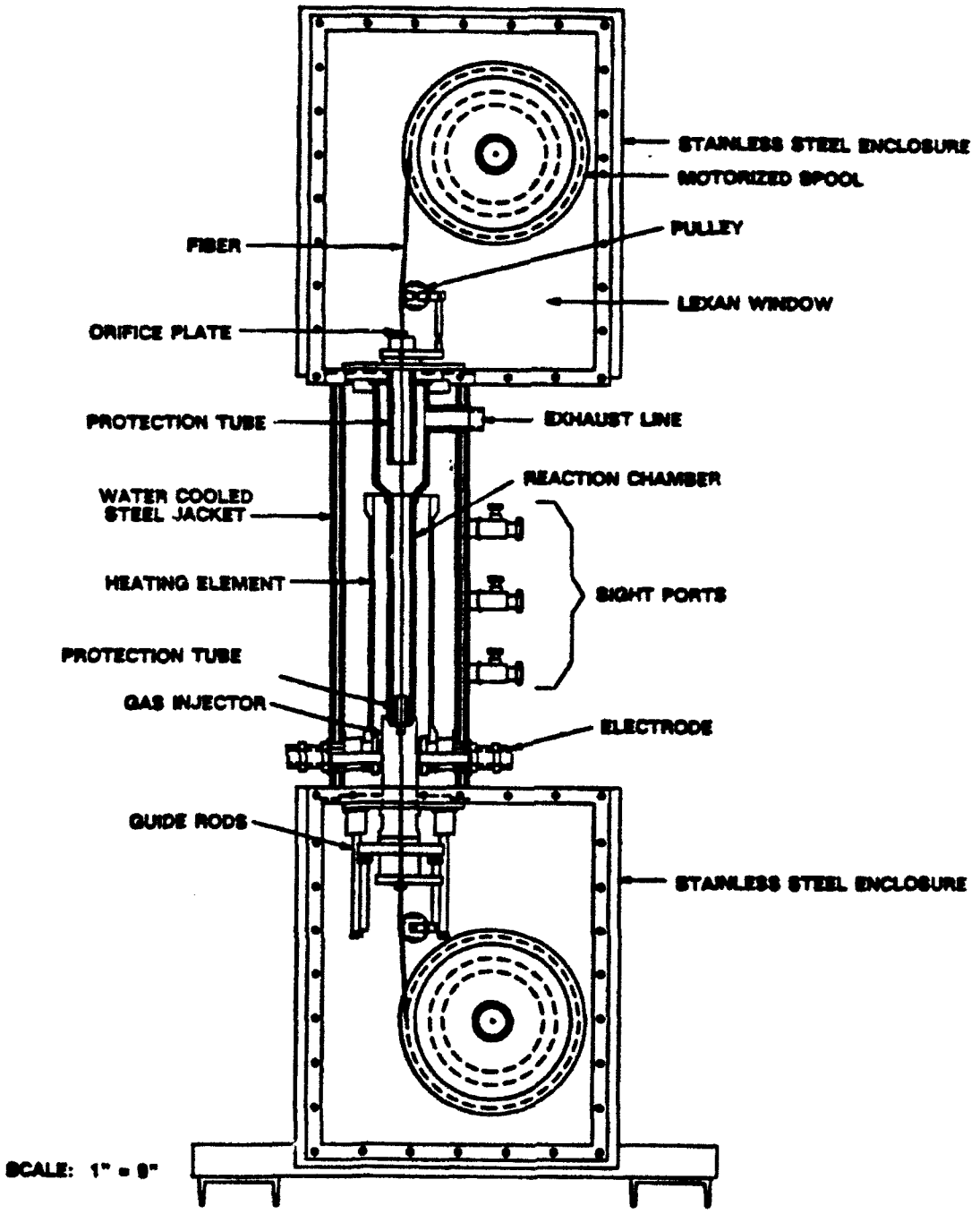


Figure 2. Schematic of the Georgia Tech continuous fiber coating system.

of 1 foot per minute is possible where the desired coating thickness is several microns. Obviously, with longer commercial size systems the pull speed is increased proportionately. Good quality SiC can be deposited at high deposition rates. This provides encouragement that high fiber pull speeds can be used.

3-2. SiC Materials Issues

SiC is a light weight material with a density of 3.21 g/cm$^3$.[40] It has a high hardness and strength and good chemical inertness. SiC exists in cubic ($\beta$) and hexagonal ($\alpha$) forms. This material has excellent resistance to oxidation to ~1650°C since a protective $SiO_2$ scale is formed. It has also been used as an oxidation protective coating for carbon-carbon composites. It is well documented[41,42] that CVD-SiC films possess superior resistance to oxidation, particularly at 1400-1700°C, and also greater resistance to creep than monolithic material prepared by sintering, hot pressing, etc. The higher purity of the CVD material probably accounts for its better properties. SiC possesses exceptionally good resistance to thermal shock.

3-3. CVD of SiC

The CVD of SiC is highly developed and well documented in the open literature and, therefore, will not be presented in any detail here. The most pertinent body of data is that on the CVI of SiC matrix composites since this mostly involves the coating and infiltration of fiber tows. This technology was recently reviewed by Lackey and Starr.[35] Their review included considerable prior work on the thermodynamic and kinetic/mass transport modeling of the CVD-SiC process.

SiC is normally deposited from either methyltrichlorosilane, $CH_3SiCl_3$, or $SiCl_4$-hydrocarbon mixtures. Typical deposition temperatures, excluding amorphous deposits prepared

for microelectronic applications, are in the range 1200-1500°C. An excess of hydrogen, over that stoichiometrically required, is normally used to react with the chlorine. The cubic $\beta$ form of SiC is normally obtained by CVD but some $\alpha$, which has only a different stacking order of the (111) planes may also be present. Monolithic and fibrous carbon are good substrates for the CVD of SiC.

## 4. MODELING

Mathematical modeling of the thermodynamic, kinetic/diffusion, and stresses developed during the fiber coating process was completed in order to assist with the deposition and to help gain insight into the coating process for future scale-up efforts.

### 4-1. Thermodynamic Modeling

During the initial 2 months of the program, thermodynamic calculations were completed for the SiC + $Si_3N_4$ deposition system. The SOLGASMIX-PV computer simulation[43] was used to study effects of temperature, pressure, and gas composition under the constraints of the conservation of mass, constant volume, and minimization of the system free energy.

Table 1 includes the species, enthalpy, and entropy used in the calculations. The thermodynamic data were obtained from Janaf[44] and Barin[45] at 1500 K. An example of the results obtained from these calculations is shown in Figure 3. The ternary processing phase diagram indicates the input gas composition and the predicted phase assemblies for a specific temperature and pressure. As shown, the two phase SiC + $Si_3N_4$ deposition region exists near the high ammonia, low methyltrichlorosilane area of the diagram. Raising the system pressure from 0.1 to 1.0 atm increased the two phase region to double the area as shown in Figure 4. For all of the calculated diagrams, single phase SiC was predicted over the majority of the area of the diagrams.

Following the change in scope of the project effort, no further thermodynamic calculations were performed. The thermodynamics of SiC deposition have been studied by several authors and further work in this area would have only duplicated earlier efforts.

Table 1. Enthalpy and entropy for the SiC + $Si_3N_4$ system.

| Species | Enthalpy kJ/mole | Entropy J/mole*K |
|---|---|---|
| Ar(g) | 0.000 | 188.427 |
| C(g) | 718.415 | 191.710 |
| CCl(g) | 500.033 | 281.784 |
| CClN(g) | 140.213 | 323.073 |
| $CCl_2$(g) | 239.895 | 354.638 |
| $CCl_3$(g) | 83.105 | 419.020 |
| $CCl_4$(g) | -85.806 | 469.835 |
| CH(g) | 591.314 | 238.318 |
| CHCl(g) | 333.341 | 312.780 |
| $CHCl_3$(g) | -102.212 | 434.832 |
| CHN(g) | 132.099 | 275.095 |
| $CH_2$(g) | 379.299 | 260.740 |
| $CH_2Cl_2$(g) | -102.442 | 391.163 |
| $CH_3$(g) | 134.662 | 277.327 |
| $CH_3Cl$(g) | -96.935 | 339.823 |
| $CH_3Cl_3Si$ | -587.547 | 568.120 |
| $CH_4$(g) | -92.553 | 279.763 |
| CN(g) | 259.742 | 253.732 |
| SiC(g) | 715.648 | 281.167 |
| $Si_2C$(g) | 519.228 | 331.239 |
| $C_2$(g) | 835.528 | 259.869 |
| $C_2Cl_2$(g) | 213.026 | 395.090 |
| $C_2Cl_4$(g) | -2.244 | 532.228 |
| $C_2Cl_6$(g) | -107.011 | 667.971 |
| $C_2H$(g) | 470.837 | 282.188 |
| $C_2HCl$(g) | 212.487 | 351.905 |
| $C_2H_2$(g) | 185.216 | 298.567 |

Table 1 (cont.) Enthalpy and entropy for the SiC + $Si_3N_4$ system.

| Species | Enthalpy | Entropy |
|---|---|---|
| | kJ/mole | J/mole*K |
| $C_2H_4(g)$ | 35.456 | 341.877 |
| $C_2Si(g)$ | 604.907 | 323.732 |
| $C_3(g)$ | 802.255 | 304.372 |
| $C_4(g)$ | 964.753 | 338.748 |
| $C_4H_{12}Si(g)$ | -319.809 | 734.499 |
| $C_4N_2(g)$ | 539.082 | 465.514 |
| $C_5(g)$ | 973.524 | 381.756 |
| Cl(g) | 125.863 | 201.323 |
| ClH(g) | -95.160 | 236.219 |
| $ClH_3Si(g)$ | -149.606 | 374.510 |
| SiCl(g) | 190.341 | 297.755 |
| $Cl_2(g)$ | 0.000 | 282.052 |
| $SiCl_2(g)$ | -175.663 | 371.590 |
| $Cl_3HSi(g)$ | -495.845 | 463.623 |
| $Cl_4Si(g)$ | -657.454 | 495.623 |
| H(g) | 234.836 | 148.299 |
| SiH(g) | 367.684 | 250.076 |
| $H_2(g)$ | 0.000 | 178.846 |
| $H_2N_2(g)$ | 207.275 | 303.767 |
| $H_3N(g)$ | -55.954 | 271.442 |
| $H_4N_2(g)$ | 91.270 | 369.884 |
| $SiH_4(g)$ | 23.548 | 317.348 |
| N(g) | 478.462 | 186.882 |
| $Si_2N(g)$ | 387.658 | 349.227 |
| SiN(g) | 365.006 | 272.180 |
| $N_2(g)$ | 0.000 | 241.880 |
| $N_3(g)$ | 421.156 | 309.238 |

Table 1 (cont.) Enthalpy and entropy thermodynamic quantities for the SiC + $Si_3N_4$ system.

| Species | Enthalpy | Entropy |
|---|---|---|
| | kJ/mole | J/mole*K |
| Si(g) | 444.803 | 202.360 |
| $Si_2$(g) | 578.658 | 294.779 |
| $Si_3$(g) | 616.934 | 364.639 |
| $C_2H_2Cl_2$ | -2.650 | 443.832 |
| $C_2H_3Cl$(g) | 27.117 | 405.563 |
| $C_2HCl_3$(g) | -2.069 | 500.435 |
| $C_3H_4$(g) | 180.900 | 349.900 |
| $C_4H_{10}$(g) | -153.740 | 604.540 |
| $C_4H_6$(g) | 225.230 | 624.490 |
| $C_4H_8$(g) | -40.961 | 463.126 |
| $C_5H_8$(g) | -165.490 | 627.090 |
| $C_6H_6$(g) | 60.337 | 538.580 |
| $C_8H_{14}$(g) | 50.860 | 941.680 |
| $C_9H_{16}$(g) | 336.520 | 363.400 |
| $Si_2H_6$(g) | 62.250 | 458.800 |
| $SiC_2$(g) | 605.240 | 323.770 |
| $SiCl_2H_2$ | -317.690 | 423.180 |
| $SiCl_3$(g) | -402.540 | 446.260 |
| C(s) | 0.000 | 33.718 |
| SiC(alph) | -71.241 | 84.410 |
| SiC(beta) | -72.851 | 84.619 |
| $ClH_4N$(s) | -265.232 | 298.149 |
| $Si_3N_4$(s) | -735.694 | 334.510 |
| Si(s) | 0.000 | 58.411 |

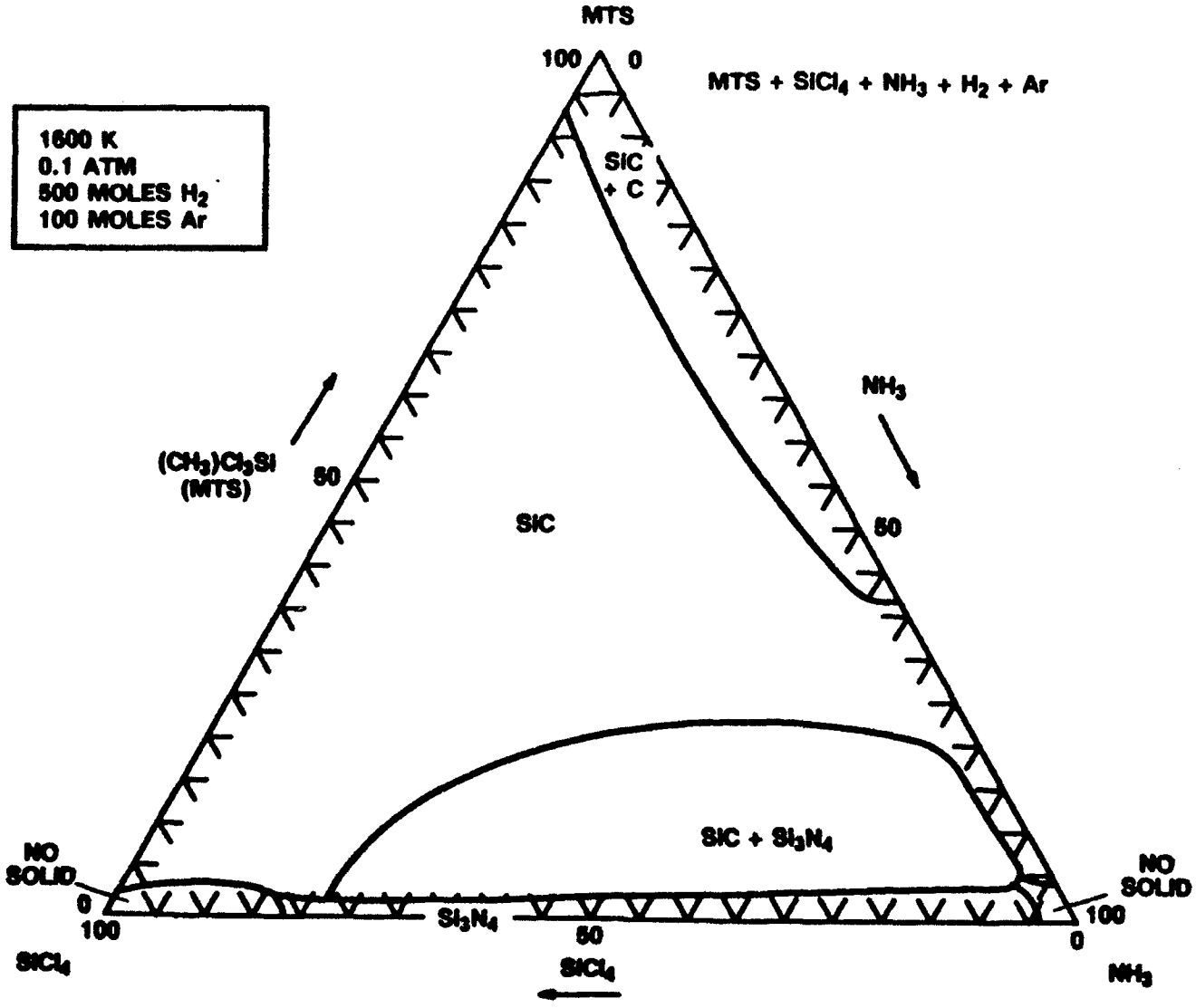


Figure 3. Ternary phase diagram for the $SiCl_4$/MTS/$NH_3$ deposition system calculated at 1600 K and 0.1 atm. Lowering the pressure reduced the SiC + $Si_3N_4$ two phase region by approximately 50%.

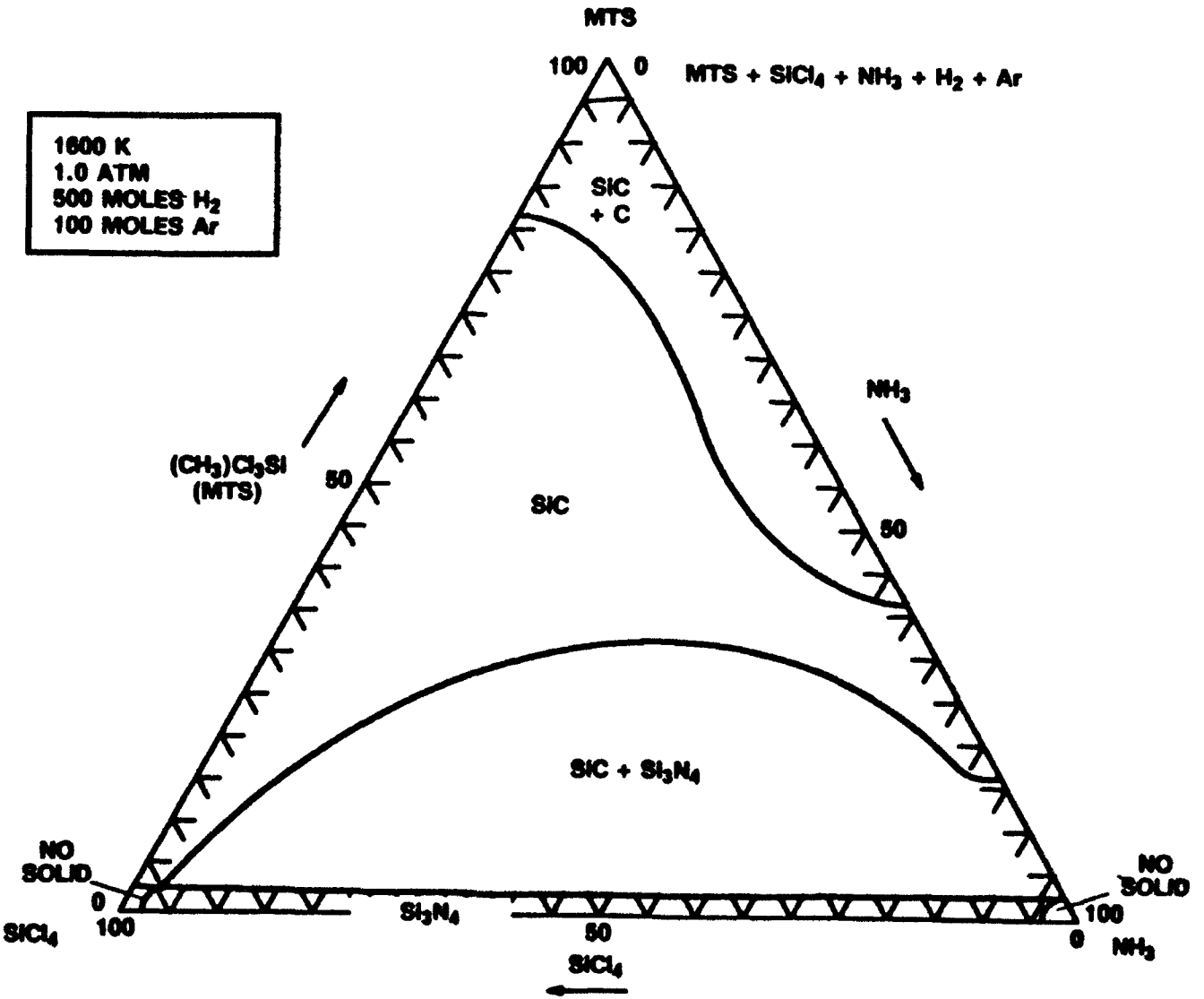


Figure 4. Ternary phase diagram for the $SiCl_4/MTS/NH_3$ deposition system calculated at 1600 K and 1 atm. A large two phase SiC + $Si_3N_4$ region was predicted to form.

4-2. Kinetic/Diffusion Modeling

A process model which helped understand the effects of the deposition and fiber coating parameters on the coating uniformity was developed. This model could be used to help scale-up the process in order to increase fiber throughput at an increased deposition rate.

a. Model Description. The model used to study the coating of multifilament fiber tows, which incorporates understanding the competition between the diffusion of a reactant gas into the fiber bundle versus the reaction rate process, was investigated by performing a differential mass balance on a cross section of a fiber bundle. Several assumptions were required in order to complete the analysis; these include assuming constant physical properties in the system, isobaric, isothermal, and steady-state processing conditions, and the chemical diffusion of a single species followed by a simple order reaction involving that chosen specie were valid. Other assumptions included that the fiber velocity was essentially zero (as compared to the gas velocity), that an effective diffusion of the specie occurred inside the fiber bundle, that no reactant depletion occurred along the length of the hot zone in the furnace, and that only one specie limited the process. The process model was modified from previous reaction/diffusion theory for catalyst conversion presented by Satterfield and Sherwood.[46]

The general form of the mass balance with a first order reaction rate is given by:

$$r^2(d^2c/dr^2) + r(dc/dr) - (K_v/D_{eff})r^2c = 0,$$

where r is the radial position within the fiber tow, c is the concentration of the limiting reactant, $K_v$ is the overall reaction rate constant, and $D_{eff}$ is the effective diffusion coefficient of species c. The equation was solved using the following boundary conditions: the concentration of the limiting reactant at the exterior surface of the fiber bundle is a known value, $c(r=R) = c_R$, and the concentration of the limiting reactant at the bundle center is a finite value, dc/dr at (r=0)

= 0. The solution to this Modified Bessel Function equation is expressed as a function of position within the fiber tow, and is given by:

$$\frac{C}{C_R} = \frac{\sum_{t=0}^{\infty} \frac{\varphi^{2t}}{\prod_{K=1}^{t} (2K)^2} \left(\frac{r}{R}\right)^{2t}}{\sum_{t=0}^{\infty} \frac{\varphi^{2t}}{\prod_{K=1}^{t} (2K)^2}}$$

The $c_R$ is the concentration of the limiting reactant at the fiber bundle surface, $\phi$ is the Thiele modulus, which, in general, is the ratio that relates the reaction rate to the diffusion as:

$$\phi^2 = K_v c^{m-1} R^2 / D_{eff}$$

where m is the reaction rate order, and t and K are counting variables for the series. Details of the solution are presented in Appendix A. For a first order reaction, the Thiele modulus reduces to $K_v R^2/D_{eff}$.

For a zero order reaction, the differential mass balance reduces to:

$$r^2(d^2c/dr^2) + r(dc/dr) = (K_v/D_{eff})r^2.$$

The solution to this equation (details presented in Appendix A) is:

$$c(r)/c_R = 1 - \phi^2/4c_R[1 - (r/R)^2]$$

The expression for the concentration gradient, $c(r)/c_R$ was programmed using BASIC (see Appendix B) and used to calculate concentration profiles for different experimental parameters on a personal computer. A flow plan of the theoretical analysis is shown in Figure 5. Geometrical factors which define the surface available for reaction (called the reaction site factor) in the fiber bundle are shown in Figure 6. The porosity present in the bundle, which

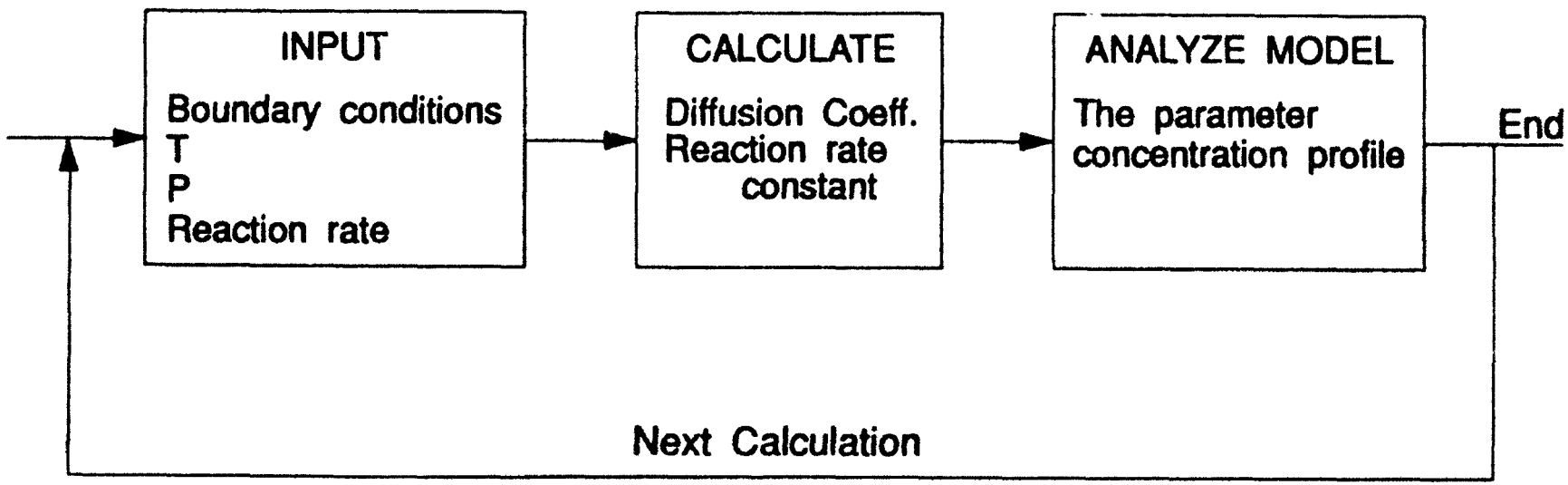


Figure 5. Flow plan for the analyses of the reaction/diffusion process.

## Actual

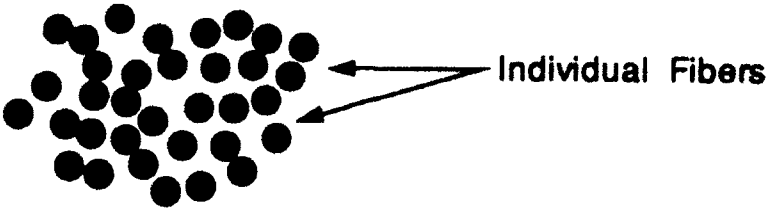


Porosity Between Fibers
( ~ 10μm )

$$\text{Porosity} = 1 - \frac{\pi r^2_{\text{fiber}} \times (\#\text{ of fibers})}{\pi R^2_{\text{tow}}}$$

## Model

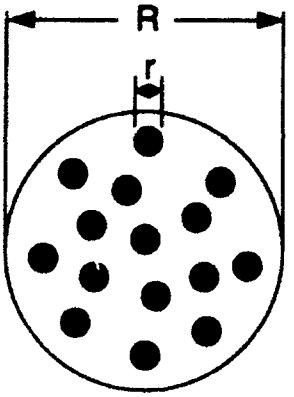


Fiber Tow Cross section

$$S_v = \text{Reaction Site Factor} \Rightarrow \frac{\text{Deposition Sites}}{\text{Area of Circle}}$$

$$= \frac{2\pi r_{\text{fiber}} \times 3{,}000}{\pi R^2_{\text{tow}}}$$

Figure 6. Physical and theoretical schematics of the geometry defined for the process model. Both the porosity and the reaction site factors were used to calculate parameters for the Thiele modulus.

was calculated from a measurement of the bundle diameter, the number of filaments in a bundle, and the fiber diameter, was typically 60-90% for the tows investigated. This corresponds to a spacing between fibers of over 10 $\mu$m, which is much larger than the mean free path of reactant gases over the range of processing variables investigated, resulting in free diffusion as opposed to Knudsen diffusion of the reactant. The diffusion coefficients were calculated using the Chapman-Enskog psuedo-binary theory for multicomponent gases at low density. (See Appendix A) Either argon or hydrogen was used as the binary partner for the reactant specie assumed to limit the deposition process.

The effective diffusion coefficient of the reactant specie through the porous fiber bundle was calculated by:

$$D_{eff} = D\theta/\tau,$$

where $\theta$ is the porosity fraction within the fiber bundle, D is the pseudo-binary free diffusion coefficient calculated from the Chapman-Enskog Theory, and $\tau$ is the tortuosity factor. The tortuosity factor was assumed to be $2^{1/2}$ -- this is an empirical correction factor obtained by "picturing the pores as randomly oriented cylinders of one fixed diameter which intersect any plane at an angle of 45°."[46]

The reaction rate expression is a function of the overall reaction rate constant ($K_v$), which is a combination of the surface reaction rate constant ($k_s$), the reaction site factor ($S_v$), and the activation energy ($E_a$) for the deposition process. These kinetic parameters were calculated or estimated from previous studies[47,48] and the current experimental work for the SiC deposition system. The calculation for the kinetic parameters was completed using deposition rate information. The activation energy for the process was determined by:

$$\text{Coating thickness/time} = k_o \exp[-E_a/kT],$$

where $E_a$ is in J/mole, k is the Boltzmann constant (8.314 J/moleK), and T is the temperature in K at a fixed reactant concentration. The activation energy corresponds to the negative slope of an Arrhenius plot of ln (deposition rate) versus 1/T. The kinetic parameters determined from the Arrhenius plot of thickness or deposition rate vs 1/T are valid for the first order rate expression as long as the concentration of reactant does not vary with temperature for the data presented.

The surface reaction rate constant was determined by calculating the surface reaction rate (moles/cm$^2$s) from the deposition rate information using the density and molecular weight of the solid formed, and dividing by the known reactant concentration, utilizing the following relationship for first order kinetics:

$$\text{rate} = k_s c \ .$$

The overall reaction rate constant, $K_v$, was determined by multiplying the surface rate constant by the geometrical site factor, $S_v$, defined in Figure 6. For a first order reaction, the units of $k_s$ are cm/s, and the units of the overall reaction rate constant are $s^{-1}$.

b. Model Input Conditions. The modeling of SiC deposition onto carbon fiber tows was completed for the Amoco T-300 fiber. For this deposition, the limiting reactant was methyltrichlorosilane (MTS), which has been used in several other modeling efforts.[47,48] Hydrogen was used as the binary component for the diffusion calculations. Figures 7 and 8 show experimental results for the SiC deposition system,[26,49] which were used to determine the first order reaction rate parameters for the model.

The deposition of SiC from MTS and $H_2$ has been extensively studied. Most of the kinetic data, and the data shown in Figures 7 and 8 are for atmospheric pressure. The activation energy has been reported from 72 to 120 kJ/mole. This large range has been attributed to the

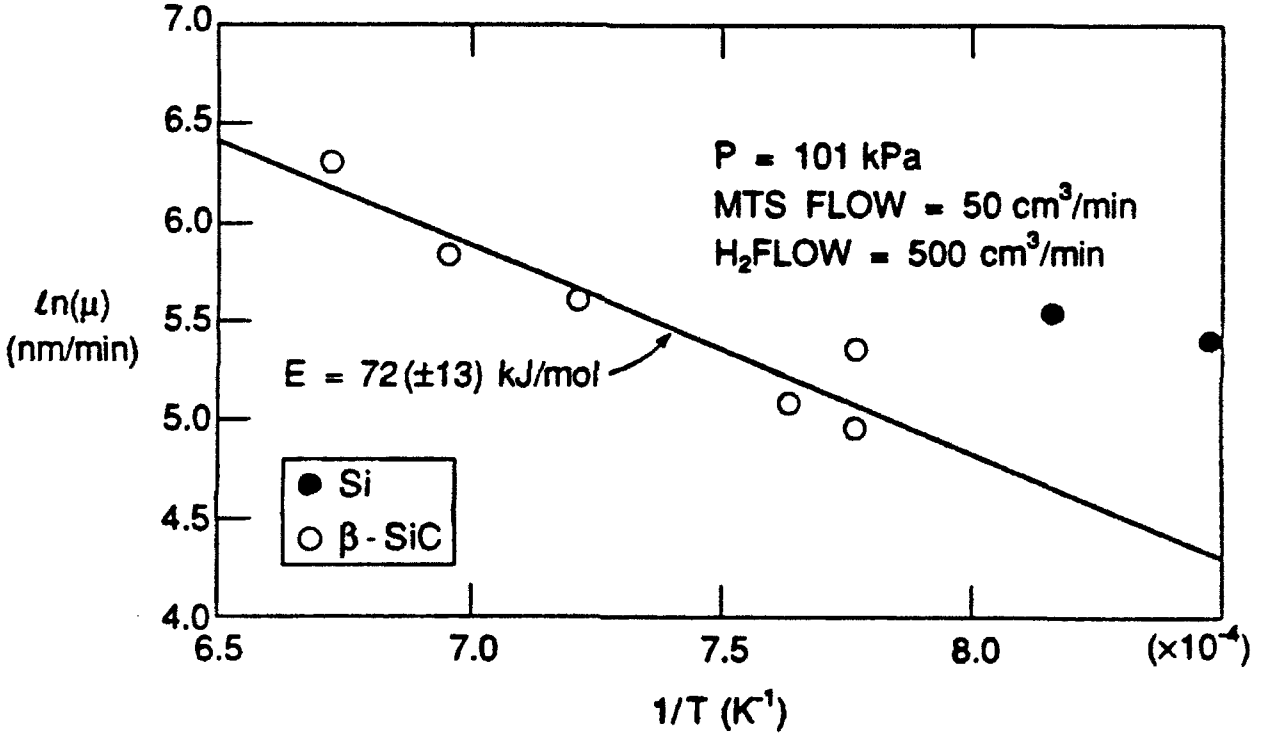


Figure 7. Arrhenius plot of deposition rate versus reciprocal temperature for SiC deposition shows an activation energy of 72 kJ/mole.

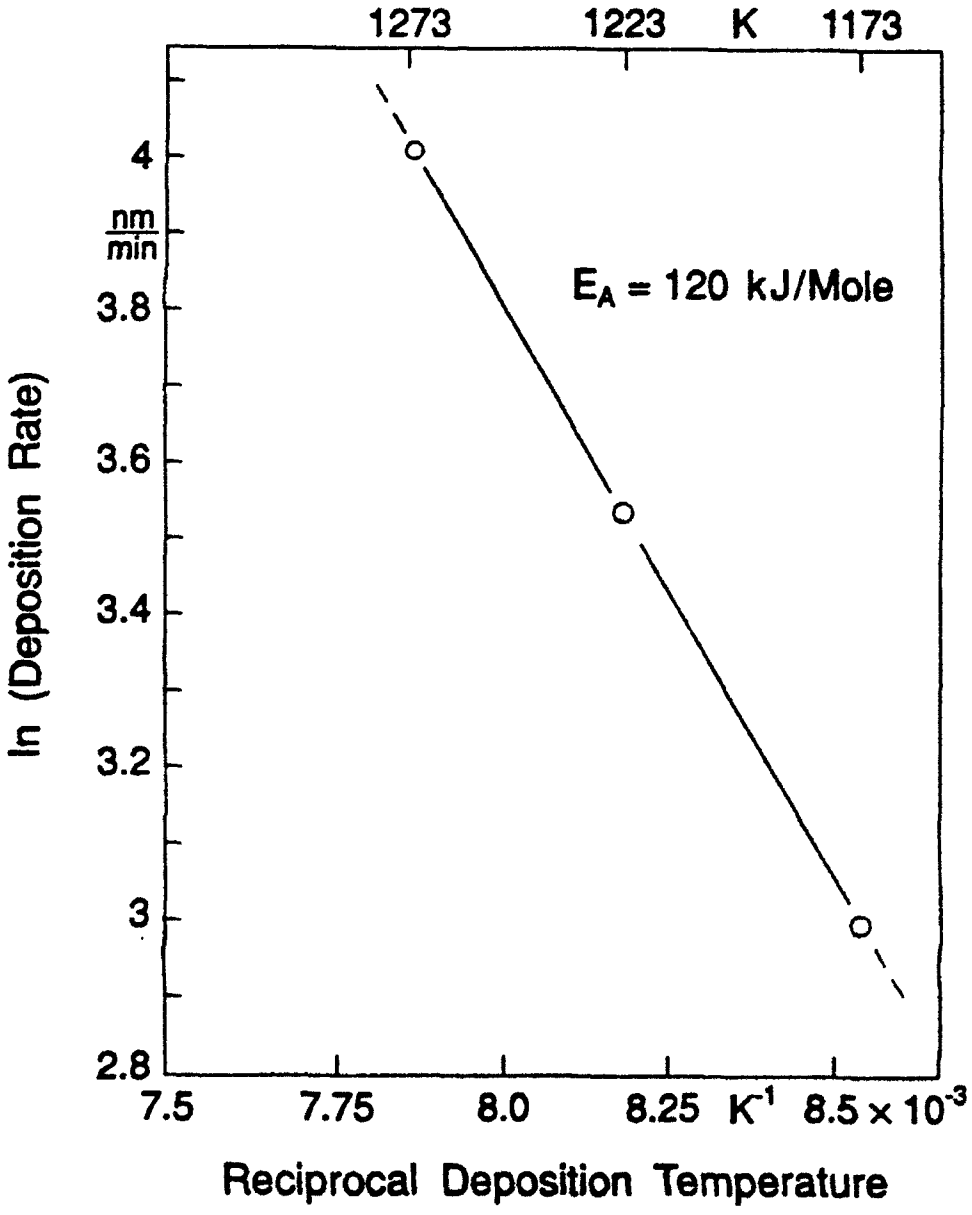


Figure 8. Arrhenius plot of experimental SiC deposition data shows an activation energy of 120 kJ/mole.

complex reaction mechanisms involved in SiC deposition chemistry. Poisoning of the reaction due to HCl formation has been definitively shown to occur. The data used for the theoretical studies span the previously reported values, although it is clear that the exact reaction rate expression is currently not understood. The rate constant was varied over a larger region ($10^{-1}$-$10^{4}$) due to the uncertainty in the theoretical model and reaction expression. The computer program input variables and ranges studied are presented in Table 2.

Table 2. Computer input parameters and ranges studied for the first order SiC deposition process.

| Parameter | Input Range |
|---|---|
| Temperature (K) | 973-1673 |
| Pressure (atm) | 0.04-1 |
| Tow Radius (cm) | 0.03-0.05 |
| Initial Concentration (moles/cm$^3$) | $10^{-8}$-$10^{-12}$ |
| First Order Rate Constant (cm/s) | $10^{-1}$-$10^{4}$ |
| Activation Energy (kJ/mole) | 72-120 |
| Mass of Limiting Reactant (g) | 158 |
| Fiber Radius (cm) | 2.8-3.5x$10^{-4}$ |
| Number of Filaments/Tow | 3000 |

c. Modeling Results. The infiltration/deposition of SiC was modeled using the input parameters presented in Table 2. A simplified first order reaction rate expression was used assuming the limiting specie was methyltrichlorosilane (MTS = $CH_3SiCl_3$). A large variation

in predicted concentration profiles was observed for this system. For example, at $E_a$ = 72 kJ/mole, $k_o$ = $10^4$ cm/s, 1673 K, and 1 atm, the concentration ratio changed from 1 at the outside of the tow to $10^{-2}$ at the center of the tow. Figure 9 shows the concentration ratio at the bundle center as a function of temperature at two different pressures.

Other model input included a range of effective diffusion coefficients of 0.4 to 21 $cm^2/s$. The overall reaction rate constant varied from 1 to $10^4$/s, and porosity changed from 70 to 89% depending on the model input conditions. Figure 10 shows the Thiele modulus versus temperature at the two activation energies used. As shown, the Thiele modulus varies from $10^{-3}$ to $10^{-1}$. Large Thiele modulus values were observed for high temperature, high pressure conditions, where the reaction rate constant times the tow radius squared was at least 10 times the effective diffusion coefficient.

d. Comparison of Experiment to Model. The experimental deposition work is summarized in a later section; however, some of the results used to validate the process model are presented here to assist in defining the kinetic parameters used for the SiC deposition. The kinetic data determined from the experimental studies were plotted as ln (coating thickness) versus 1/T in order to validate the range of activation energies used in the model. This plot is shown in Figure 11, and gives an activation energy of 113 kJ/mole, which is within the range studied. The kinetic information was obtained by fixing the pressure, fiber pull speed, hydrogen and inlet MTS concentration. The majority of processing conditions simulated by the model predicted a uniform concentration profile throughout the tow. High temperature, high pressure conditions which used the faster kinetic parameters did result in a drop in expected reactant concentration as a function of position. For larger fiber spreading values a uniform deposition would be anticipated.

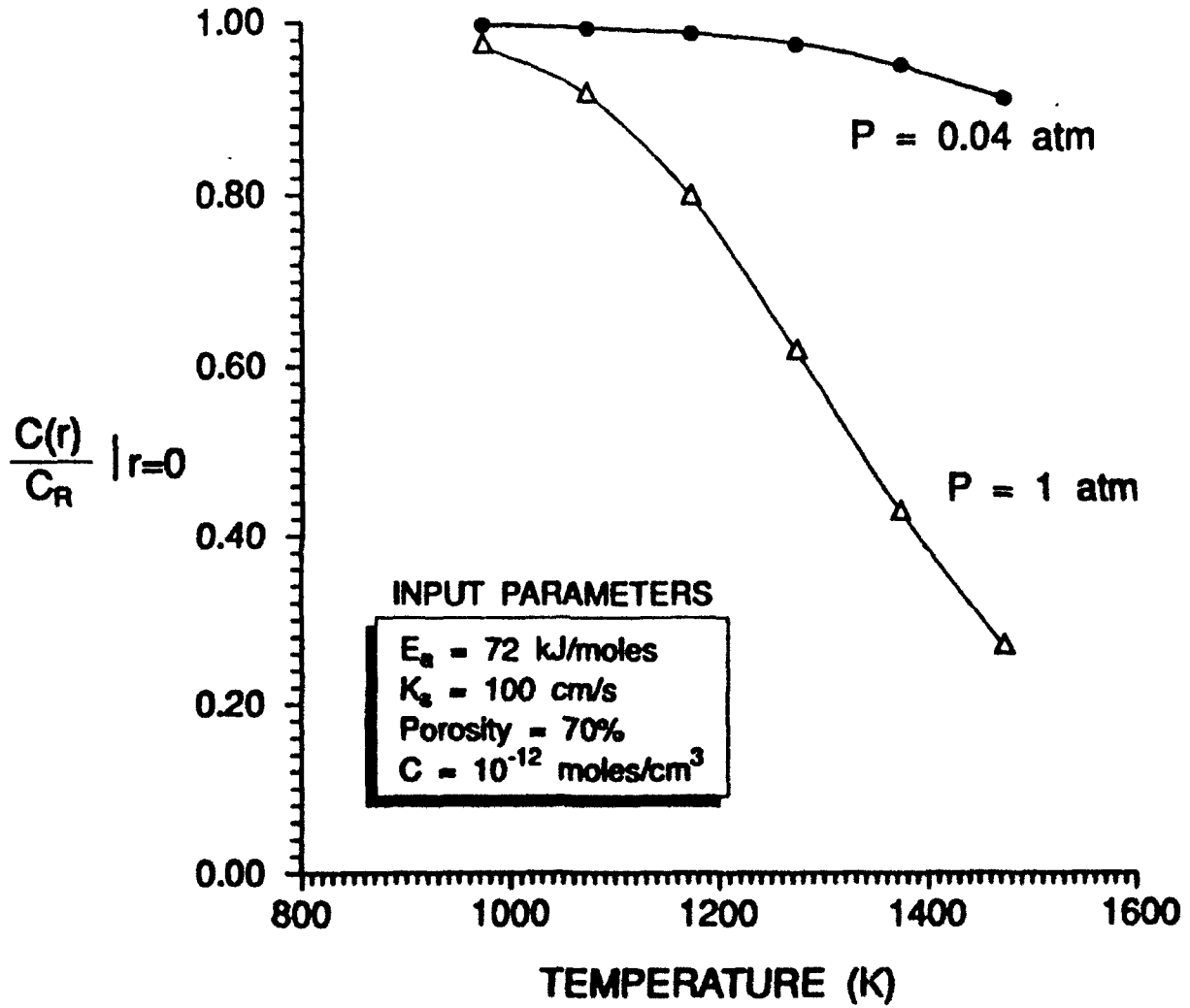


Figure 9. Concentration ratio at the fiber tow center versus temperature at two different pressures for the SiC system.

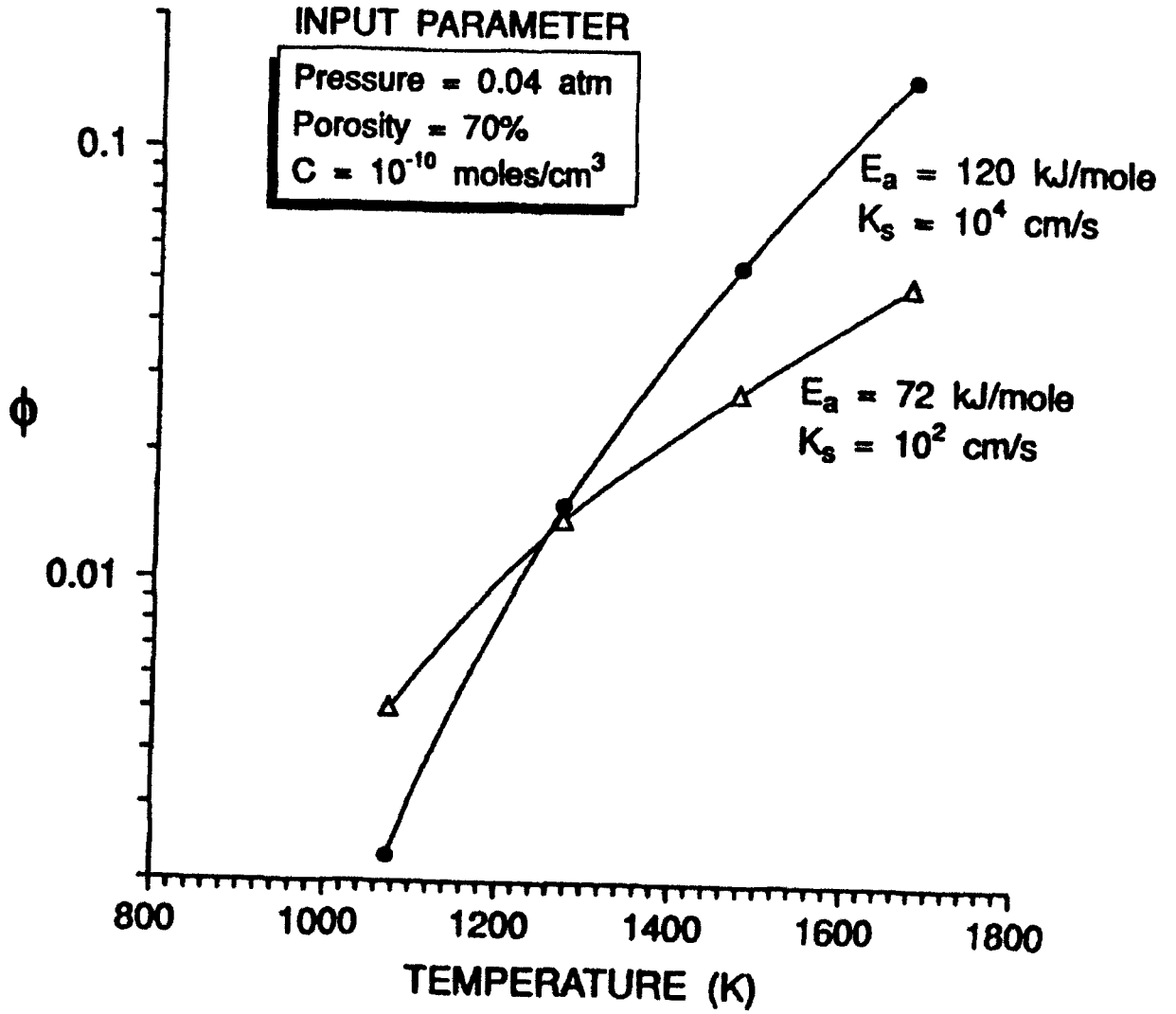


Figure 10. Thiele modulus versus temperature at the two activation energies used to model SiC deposition.

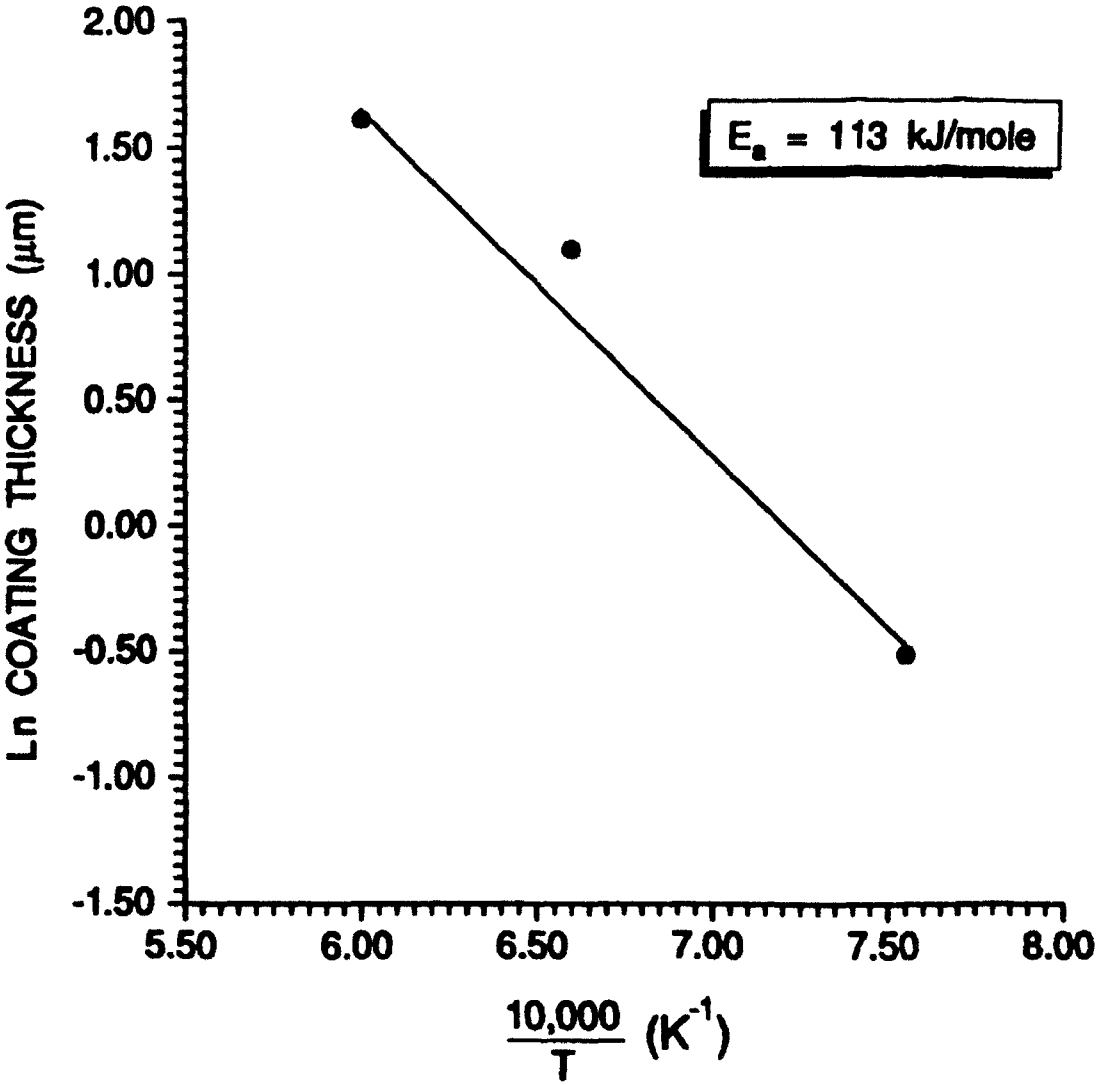


Figure 11. Ln coating thickness versus 1/T for the SiC deposition study. The linear relationship indicates an activation energy of 113 kJ/mole.

A variation in coating thickness was observed for a run which was conducted at 1350°C, 3 ℓ/min $H_2$, and 7 g/min MTS flow rate. SEM micrographs from this run are shown in Figure 12. A plot of the predicted coating thickness (converted from the concentration profile) versus radial position is shown in Figure 13. The experimentally observed coating thickness is also shown; both values decrease into the fiber tow.

One problem which is not explained by the model is the overcoating, or blocking of the diffusion paths for samples with fast reaction compared to diffusion. When the Thiele modulus is greater than ~10, the system operates similar to a chemical vapor infiltration process. If the reaction/diffusion model predicts a large concentration gradient, it is more likely that the fiber tow will be "canned" by the solid deposit, with very little or no coating on the inner filaments.

In this model study, the following general relationships were found: 1. Complete infiltration was favored by low temperture, low pressure, high activation energy, and low reactant concentration conditions. 2. The Thiele modulus was controlled by the reaction rate, i.e., the kinetic parameters used controlled the value of the modulus. Diffusion coefficients were found to vary from ~$10^{-1}$-10 $cm^2/s$ whereas the reaction rate constant varied over several orders of magnitude. Finally, the initial fiber also influenced the ability to completely infiltrate the tow; small diameter filaments and a small number of filaments were preferred for complete infiltration.[50]

4-3. Stress Modeling

The modeling of stresses which would develop in a coated fiber during cooling due to thermal expansion mismatch or fiber or coating anisotropy were studied using equations presented by Hsueh, et al.[51] The results from the analysis are being published as part of a

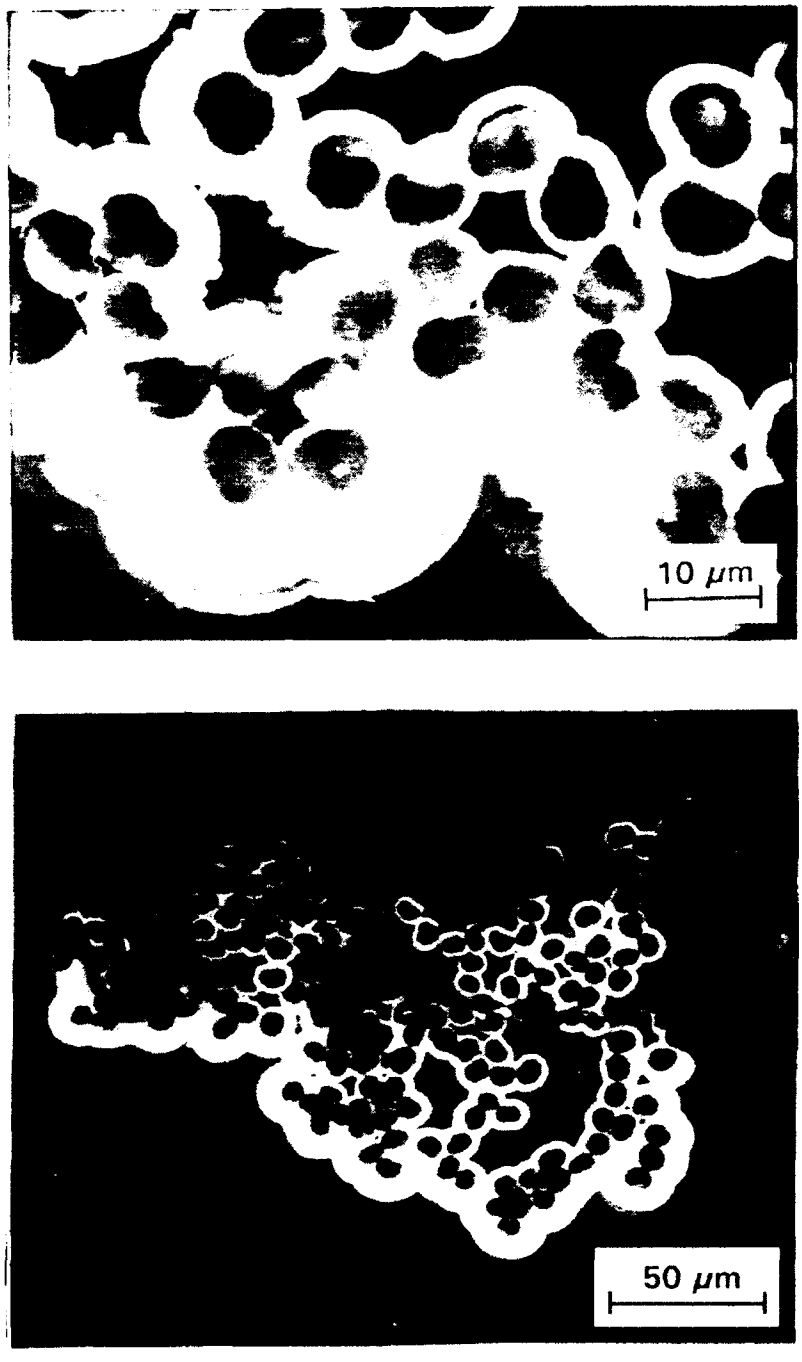


Figure 12. SEM micrograph for a SiC coating which shows a coating thickness variation as a function of radial position.

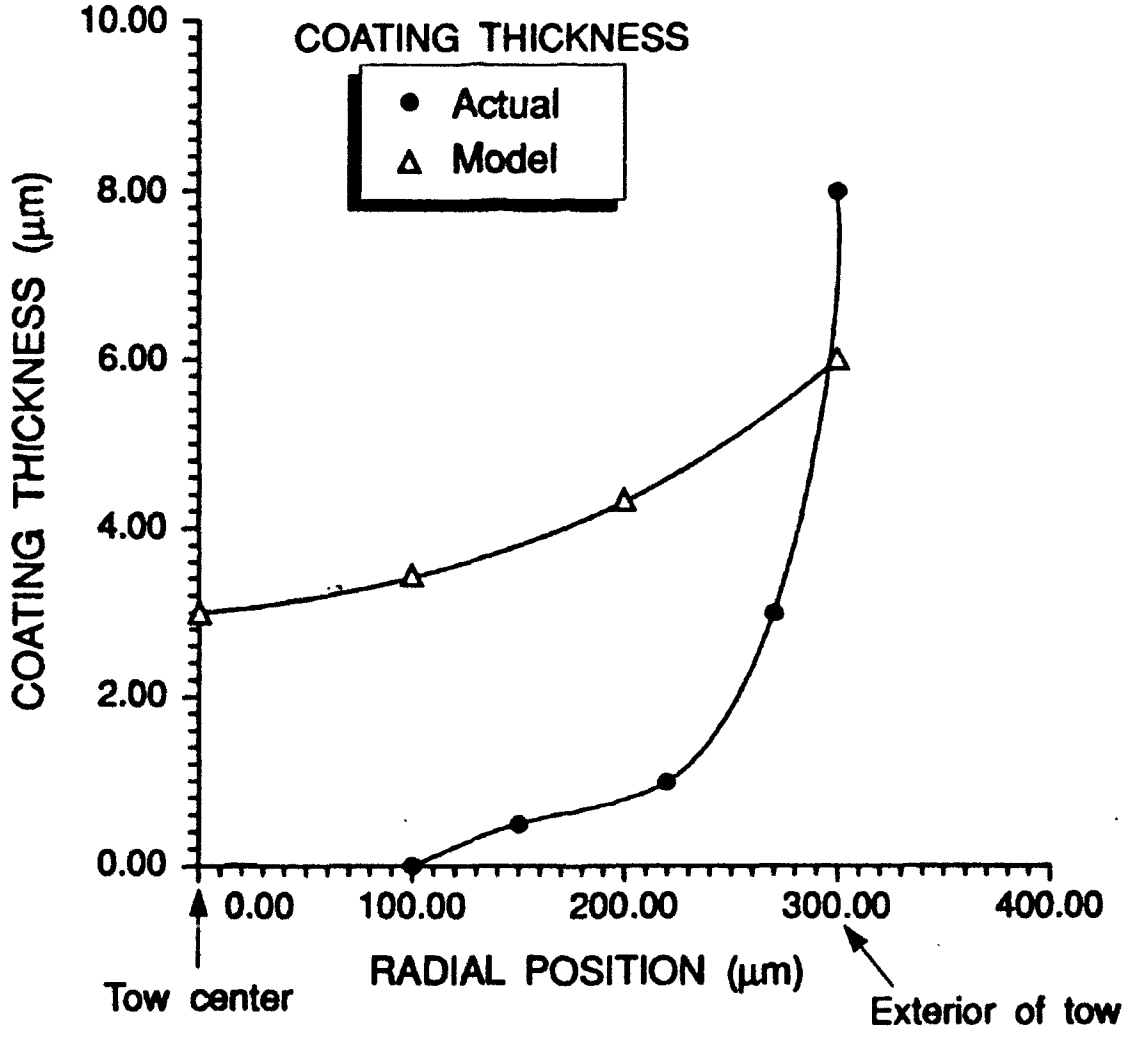


Figure 13. Predicted and experimental coating thickness versus radial position for SiC deposition on carbon fibers. Both profiles decrease as they move toward the center of the tow.

larger effort on understanding fiber coating stresses.[52] Axial, tangential, and radial stress components were compared for SiC coatings deposited onto various commercial carbon tows. The goal of this theoretical work was to help guide carbon substrate selection in order to minimize any fiber/coating damage. The effect of coating thickness and bending on the maximum axial stress was also considered for the fiber/coating pairs.

Table 3 contains the material properties required for the stress calculations. Calculated stresses were as high as 2.5 GPa but were typically less than about 0.5 GPa. The stresses calculated are the sum of the thermal expansion mismatch and the anisotropic stresses. Figure 14 defines the geometry and stress components used in the model. As shown in Table 3, most carbon fibers contain a high level of anisotropy in their coefficients of thermal expansion (CTE's); i.e., the CTE in the radial direction differs significantly from that for the axial direction.

Table 3. Physical and mechanical properties of fibers and coatings.[52]

| | Thermal Expansion (300-150CK) | | Young's Modulus | Poisson | Tensile Strength | Fiber Radius |
|---|---|---|---|---|---|---|
| | Radial | Axial | (GPa) | Ratio | (GPa) | ($\mu$m) |
| | ($10^{-6}$ $K^{-1}$) | | | | | |
| Fibers | | | | | | |
| Carbon | | | | | | |
| T-50 | 6.70 | 0.352 | 391 | 0.2 | 2.8 | 2.8 |
| T-300 | 8.85 | 0.932 | 232 | 0.2 | 3.6 | 2.8 |
| Coating | | | | | | |
| SiC | 5.5 | 5.5 | 428 | 0.2 | 1-2.4 | |

In order to help judge which fiber-coating combination would not develop catastrophic stresses due to thermal expansion mismatch, comparison calculations were completed for coating thicknesses in the range of 0 to 5 $\mu$m for the T-50 and T-300 fibers. Figure 15 shows the

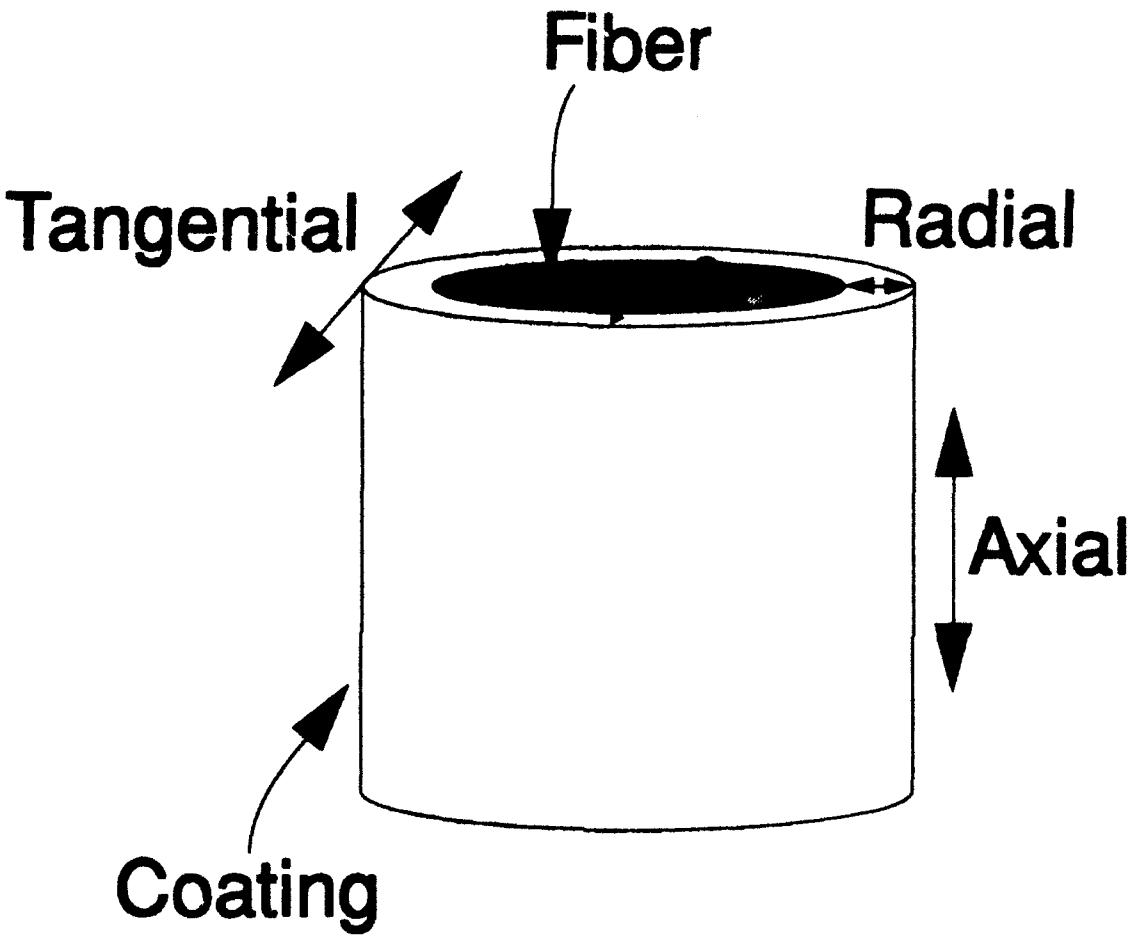


Figure 14. Definition of orientations for stress calculations.

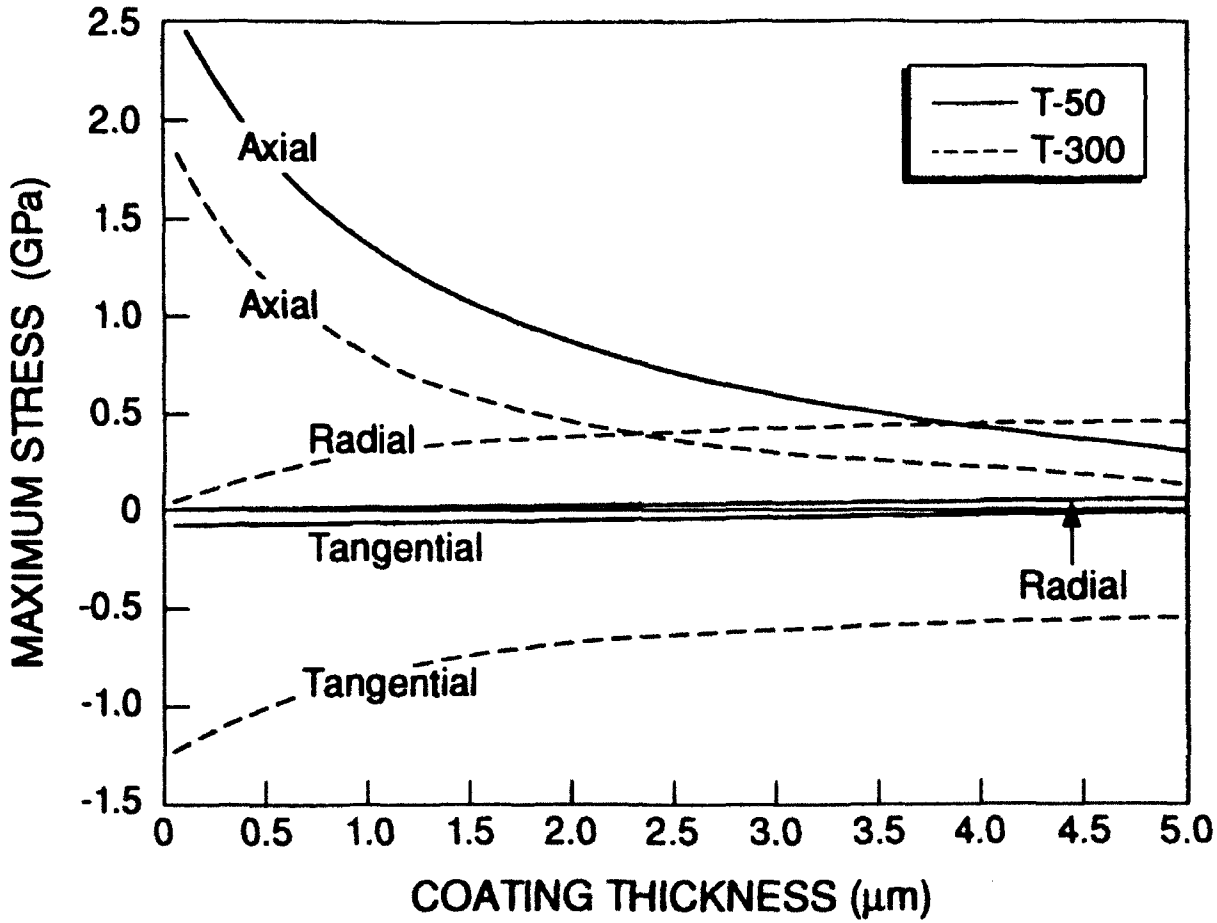


Figure 15. Maximum magnitude of stress components as a function of coating thickness for two carbon fibers. Tensile stress is positive; compressive stress is negative.

maximum radial, axial, and tangential stresses for both fibers as a function of coating thickness. It can be seen from Figure 15 that the axial stresses in the coating for C(T-50)-SiC systems are greater than corresponding stresses in C(T-300)-SiC systems for a range of coating thickness from 0 to 5 $\mu$m. For the target coating thickness of 5 $\mu$m, the stresses are well below the strength of CVD-SiC ($\sim$ 2 GPa). It should be mentioned that cracked coatings were never observed experimentally even when the coating thickness was 1 $\mu$m or less.

Another analysis was completed which evaluated the maximum axial stresses for both no bending and bending states of the fiber. Figure 16 shows the maximum axial stress as a function of coating thickness for the no bending case for a T-50 fiber. As shown, for a coating thickness of 5 $\mu$m, which is desired for the development of SiC fibers, a stress of 0.25 GPa is expected. This is considered an acceptable stress for the fiber/coating system. Figure 17 shows the effect of bending radius as a function of coating thickness for the maximum axial stress. As the bending radius decreases, the axial stress increases. Assuming a strength of 2 GPa, these results indicate that a fiber with a 5 $\mu$m thick coating could be bent to a radius of 0.2 cm. This is sufficient to permit weaving of cloth.

These analyses were useful in determining which fiber was preferred for the deposition work. The experiments were performed using the T-300 fiber since the tensile stresses were lower in the 1 to 5 $\mu$m coating thickness range as compared to the T-50 fiber. Also, the T-300 fiber is available without sizing and not twisted.

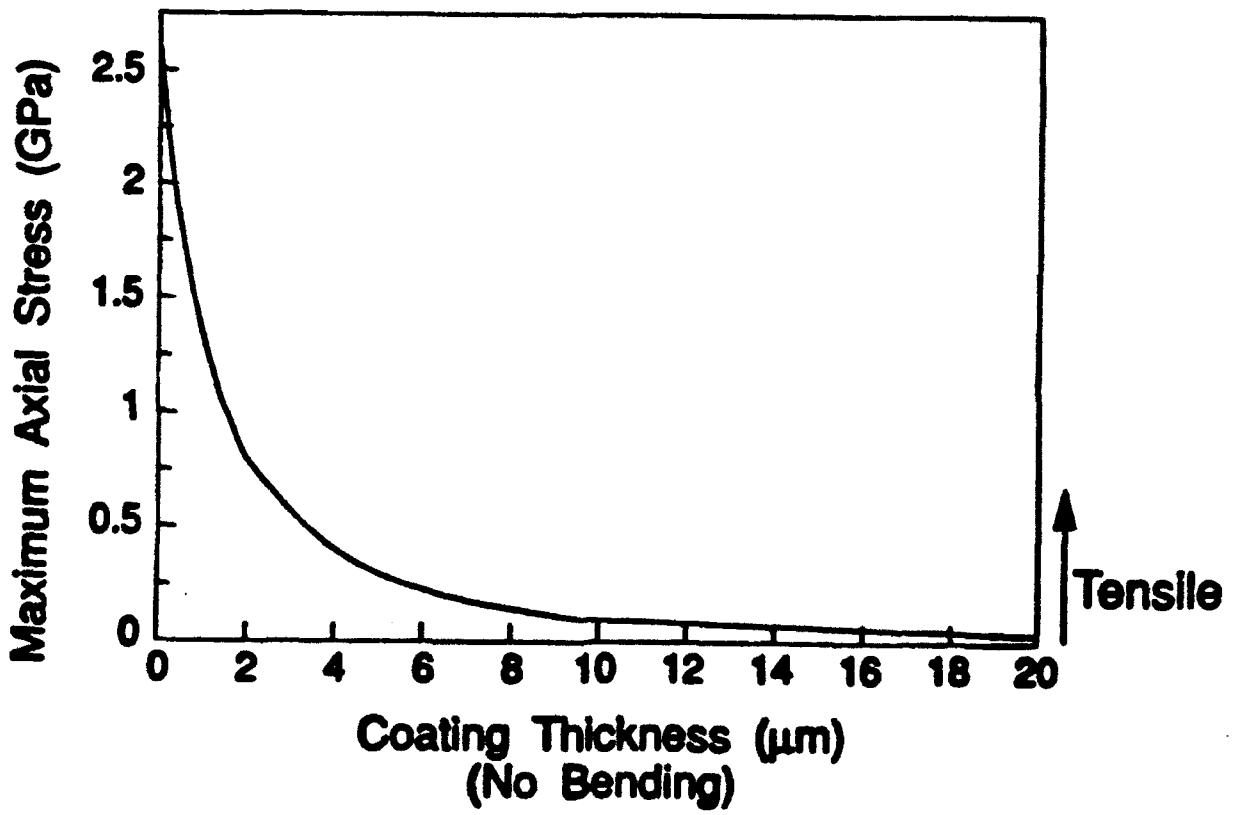


Figure 16. The maximum axial stress for the no-bending case shows that for a 5 $\mu$m thick SiC coating, an acceptable stress is predicted.

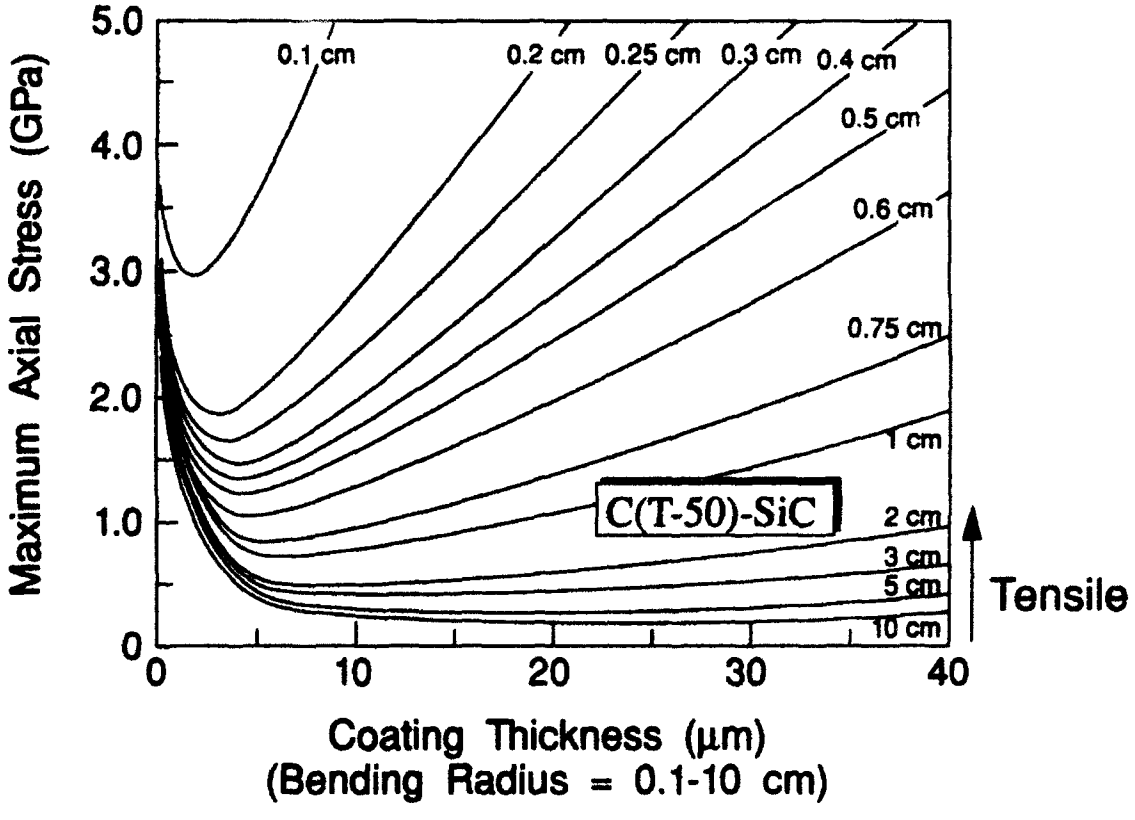


Figure 17. Maximum axial stress in the coating as a function of coating thickness for SiC coatings on Amoco T-50 carbon fiber.

## 5. PROCESSING STUDY

Over 200 deposition experiments were performed during this 15 month effort. The study of SiC deposition on fiber tows, and more importantly, the study of fiber spreading techniques were completed.

### 5-1. Initial Deposition

Early in the program the objective was to codeposit SiC and $Si_3N_4$. Using the thermodynamic equilibrium calculations from the SOLGASMIX-PV computer simulation program, 15 deposition runs were performed, which varied temperature and pressure in the regions of interest (high $NH_3$, low MTS concentrations). At high pressures, SiC powder was formed. At lower pressures, felt-like, greyish black films were deposited on polycrystalline alumina, graphite flat substrates, and Amoco T-300 carbon fiber. A four-run study varying the $SiC/Si_3N_4$ ratio by incrementally increasing the MTS concentration was completed which resulted in the two-phase deposition of SiC + $Si_3N_4$.

Initial work coating SiC on carbon fiber included 10 runs comparing sized to unsized fiber. The unsized fiber was easier to spread than the sized fiber, allowing better deposition and infiltration of the SiC on the individual filaments of the tow. The use of twisted fiber was also avoided due to obvious spreading problems. The fiber spreader used in these experiments consisted of two rollers with narrow slits through which argon gas flowed (Figure 18). More description of this and other fiber spreaders are included in a later section. X-ray diffraction was used to verify the prescence of SiC on the fiber tow.

More experiments to coat SiC on carbon fiber concentrated on depositing thick, uniform coatings around each filament of a fiber tow. Fifteen experiments were completed on unsized Amoco T-300 fiber (3000 filaments/tow) at 1250°C, 0.1 atm, at a fiber pull speed of 10

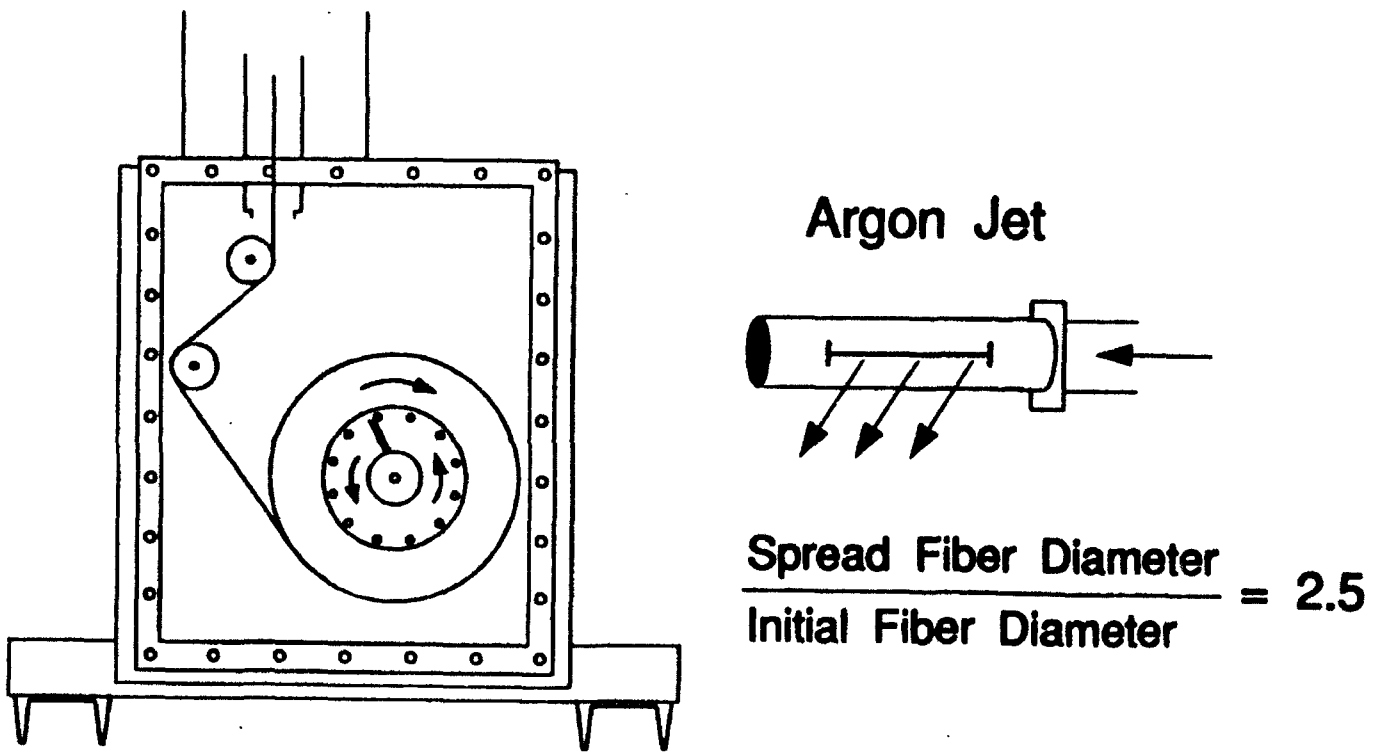


Figure 18. Schematic of the fiber spreading attachments on the continuous fiber coater. The fiber spreads due to the friction on the curved surface, and due to the argon jet through the narrow slit.

cm/min. The spreading device described previously was used. Figure 19 shows a uniform coating of SiC on the Amoco fiber. Experiments completed at higher pressures (0.5 atm) resulted in thick but nonuniform coatings. Further deposition work varied the amount of MTS from 3 to 7 g/min. The lower MTS concentration produced thin layers of SiC (0.25 - 0.5 $\mu$m). In order to achieve the desired thicker coatings, the MTS flow rate was increased to 5 g/min.

Initial tensile tests of 6 cm gauge length filaments of uncoated Amoco T-300 fiber resulted in strength values between 2.5 and 3.8 GPa. These values agree with the reported strength value of 3.65 GPa from Amoco. Tensile tests on some of the initial coated fibers with 1 $\mu$m of SiC yielded strength values of approximately 1 GPa.

5-2. Statistical Study

a. Design. At this point, a box statistical study was designed (Figure 20) to assist in defining the optimal conditions for depositing SiC on carbon fibers. This study centered around deposition conditions of 1250°C, 2.5 $\ell$/min $H_2$, and 5 g/min MTS flow rate. The experiments varied temperature from 1050°C to 1450°C, $H_2$ flow rate from 1.5 to 3.5 $\ell$/min, and MTS flow rate from 1 to 9 g/min. A fiber spreading device was employed which cyclically applied and released tension on the carbon fiber at 1 second intervals. The fiber pull rate was 10 cm/min, and the pressure was 100 torr. Scanning electron microscopy, weight gain, and x-ray diffraction were used to characterize the fibers. The strength of the coated fibers was measured by tensile testing, and the percent agglomeration was observed from SEM micrographs. The study focused on strength values and percent agglomeration as a function of the processing variables.

b. Property-Processing Correlations. A summary of the experimental study and response data are shown in Table 4. This table includes run number, run conditions, operating

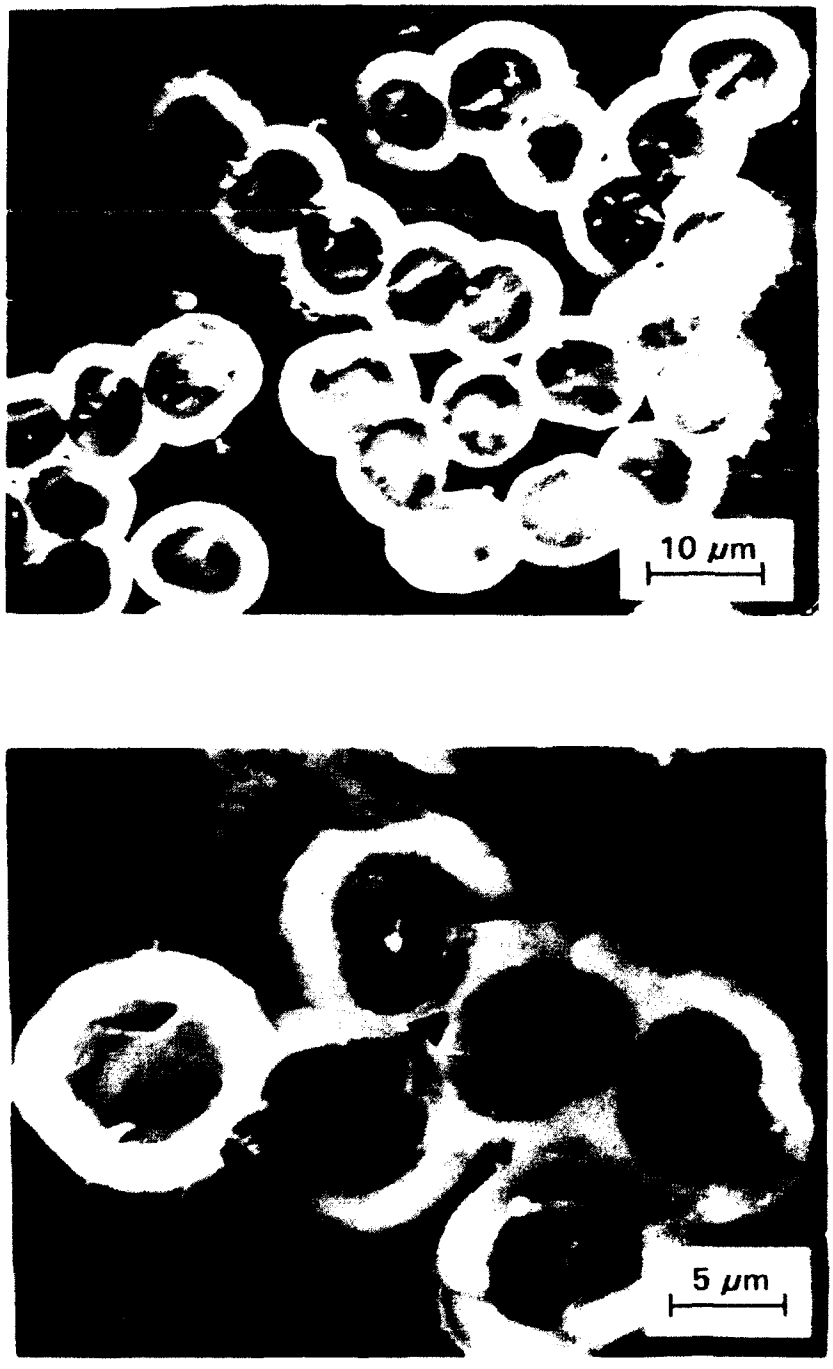


Figure 19. A 3 μm SiC film was uniformly deposited at 1250°C, 0.1 atm on fiber moving at 20 cm/min.

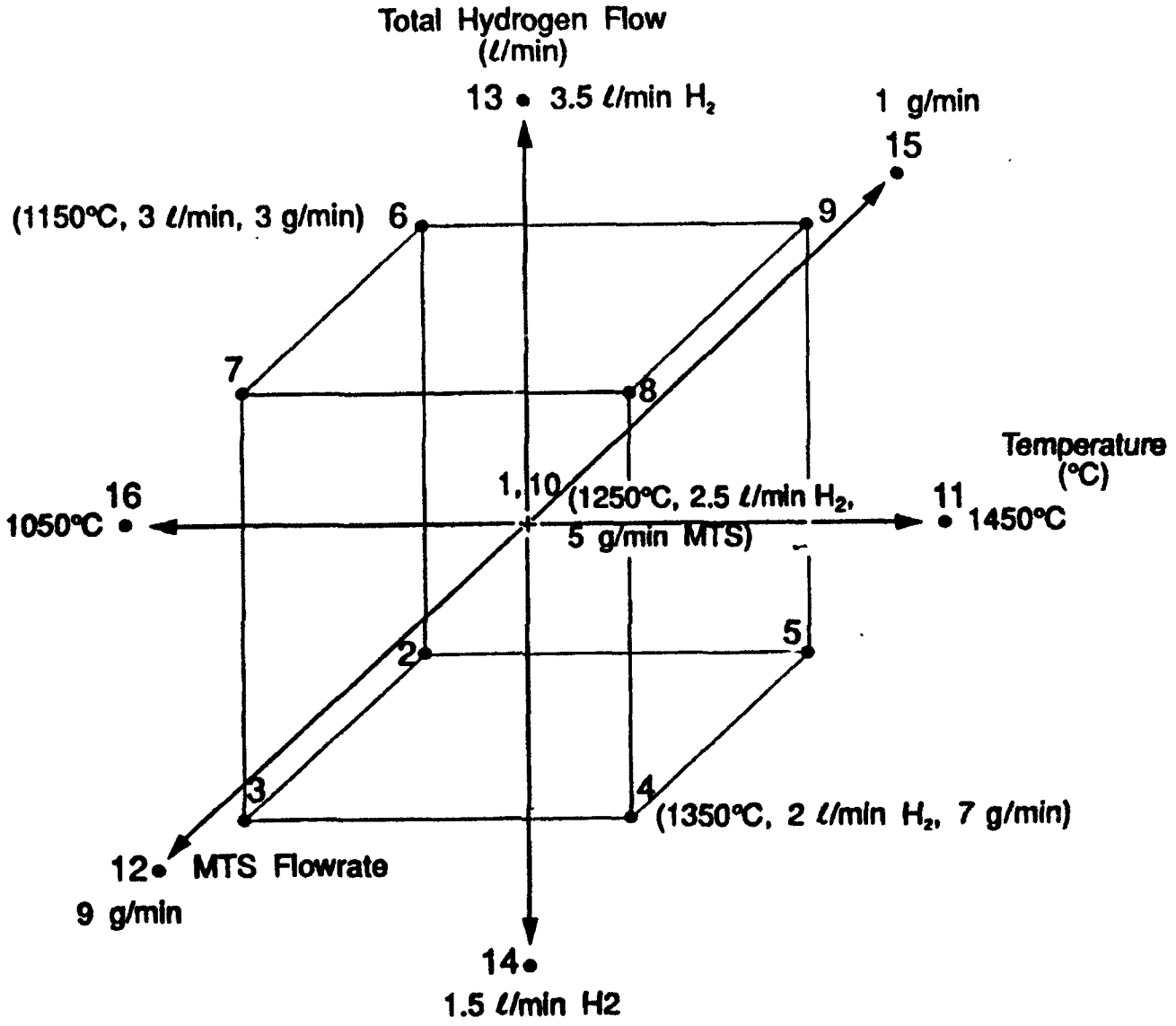


Figure 20. Schematic of the statistical processing design used to study SiC deposition. Statistical design of experiments is described in many texts such as Norman L. Johnson and Fred C. Leone, "Statistics and Experimental Design in Engineering and the Physical Sciences", Vol. 2, John Wiley & Sons, NY, 1976.

Table 4. Operating conditions and fiber attributes for the statistical processing study for SiC deposition.

| Run # | RUN CONDITIONS | | | | | | Operating pressure (torr) | Tensile Strength average range (GPa) | Weight of 6" coated fiber (g) | Thickness (μm); % agglomeration |
|---|---|---|---|---|---|---|---|---|---|---|
| | T desired (°C) | T actual (°C) | $H_2$ desired (l/min) | $H_2$ actual (l/min) | MTS desired (g/min) | MTS actual* (g/min) | | | | |
| Uncoated fiber | - | - | - | - | - | - | - | - | 0.0290 | |
| SC-18 | 1050 | 1050 | 2.5 | 2 | 5 | 1.7 | 150 | $\overset{1.67}{0.82 \rightarrow 2.35}$ | 0.0336 | <1; 0 |
| SC-19 | 1150 | 1150 | 3 | ~2.8 | 3 | 2.9 | 175 | $\overset{1.33}{0.77 \rightarrow 2.35}$ | 0.0356 | <1; 0 |
| SC-20 | 1250 | 1250 | 1.5 | 1.5 | 0 | 0 | 125 | $\overset{1.95}{1.35 \rightarrow 2.36}$ | - | - |
| SC-21 | roomT | roomT | 0 | 0 | 0 | 0 | 760 | $\overset{2.68}{1.91 \rightarrow 3.1}$ | - | - |
| SC-22 | 1250 | 1250 | 2.5 | 2.5 | 5 | 5.3 | 155 | $\overset{1.04}{0.83 \rightarrow 2.02}$ | 0.062 | 4; 30 |
| SC-23 | 1450 | 1400 | 2.5 | 2 | 3 | 1.8 | 100 | $\overset{1.35}{1.08 \rightarrow 2.07}$ | 0.073 | 5; 90 |
| SC-24 | 1150 | 1150 | 2 | 2 | 3 | 1.6 | 90 | $\overset{1.62}{0.75 \rightarrow 2.51}$ | 0.033 | <1; 0 |
| SC-26 | 1350 | 1350 | 3 | 3 | 7 | 8.0 | 125 | $\overset{5.68^{**}}{3.11 \rightarrow 8.52}$ | 0.093 | 2; 90 |
| SC-27 | 1350 | 1350 | 2 | 0.9 | 7 | 7.9 | 110 | $\overset{3.62^{**}}{2.26 \rightarrow 3.82}$ | 0.132 | 7; 90 |
| SC-28 | 1350 | 1350 | 2 | 2 | 3 | 2 | 120 | $\overset{2.22}{1.82 \rightarrow 2.61}$ | 0.047 | 2; 50 |
| SC-29 | 1250 | 1250 | 2.5 | 2.5 | 5 | 7.3 | 140 | $\overset{0.98}{0.52 \rightarrow 1.62}$ | 0.099 | 3; 50 |
| SC-30 | 1350 | 1350 | 3 | 2.8 | 3 | 1.8 | 160 | $\overset{1.74}{1.35 \rightarrow 2.16}$ | 0.034 | <1; 0 |
| SC-31 | 1150 | 1150 | 3 | 2.8 | 7 | 7.2 | 175 | $\overset{1.09}{0.44 \rightarrow 1.36}$ | 0.058 | 1.5; 80 |
| SC-32 | 1150 | 1150 | 2 | 2 | 7 | 7.4 | 200 | $\overset{1.59}{0.91 \rightarrow 2.67}$ | 0.040 | <1; 60 |
| SC-33 | 1250 | 1150 | 3.5 | 3.5 | 3 | 3.475 | 200 | $\overset{1.19}{0.41 \rightarrow 1.86}$ | .0337 | <1; 0 |
| SC-34 | 1250 | 1150 | 2.5 | 2 | 1 | 0.875 | 75 | $\overset{0.85}{0.62 \rightarrow 1.42}$ | .0354 | <1; 0 |
| SC-35 | 1250 | 1150 | 2.5 | 2 | 9 | 6.31 | 100 | $\overset{0.58}{0.46 \rightarrow 0.73}$ | .0506 | 4; 90 |
| SC-36 | 1250 | 1150 | 1.5 | 1.5 | 3 | 1.43 | 100 | $\overset{155}{1.04 \rightarrow 2.20}$ | .0320 | <1; 0 |

*The actual MTS flow rate was determined by weighing the vaporizer before and after each run.
**Tensile samples had 2cm gauge lengths.

pressure, average tensile strength values, and weight of the coated fibers. Both thin and thick coatings were deposited (Figure 21); the thickness ranged from 0.1 to 7 $\mu$m. Surface roughness was also evaluated; smooth coatings are expected to result in higher strength fibers due to the lack of failure initiating flaws. The morphology range of the coatings from the study is shown in Figure 22. The nodular films were deposited at high MTS concentrations. Results from this characterization were used to correlate processing parameters to the fiber attributes.

Tensile strength of the filaments was measured using an Instron model 1331 tensile testing machine equipped with pneumatic grips to pull the samples to fracture at a rate of 0.031 cm/s. At least 10 fibers were tested at a gauge length of 6 cm unless otherwise noted. Some of the samples were extremely brittle and could not be separated into individual filaments; shorter gauge lengths were used to evaluate the strength of these fibers. The strengths generally ranged between 1 and 2 GPa for the fibers prepared in the statistical study. Fibers prepared in later work had tensile strengths above 2 GPa. Figure 23 presents the tensile strength versus coating thickness, and Figure 24 shows the tensile strength versus deposition temperature. The uncertainties shown in the figures represent the range. The strength appears to generally decrease with increasing coating thickness and temperature although the trends were not statistically significant.

Table 5 summarizes the general results from the multiple regression analysis of the data, indicating the response variable and the processing parameters which had significant positive or negative affects on the final properties. Multiple regression analysis (see Appendix C) showed, with greater than 99% confidence, that the weight gain of coated fiber tows had a large positive correlation with both temperature and MTS flow rate, i.e., weight gain increased with increasing temperature and MTS flow rate. There was a 94% confidence that hydrogen flow rate had a

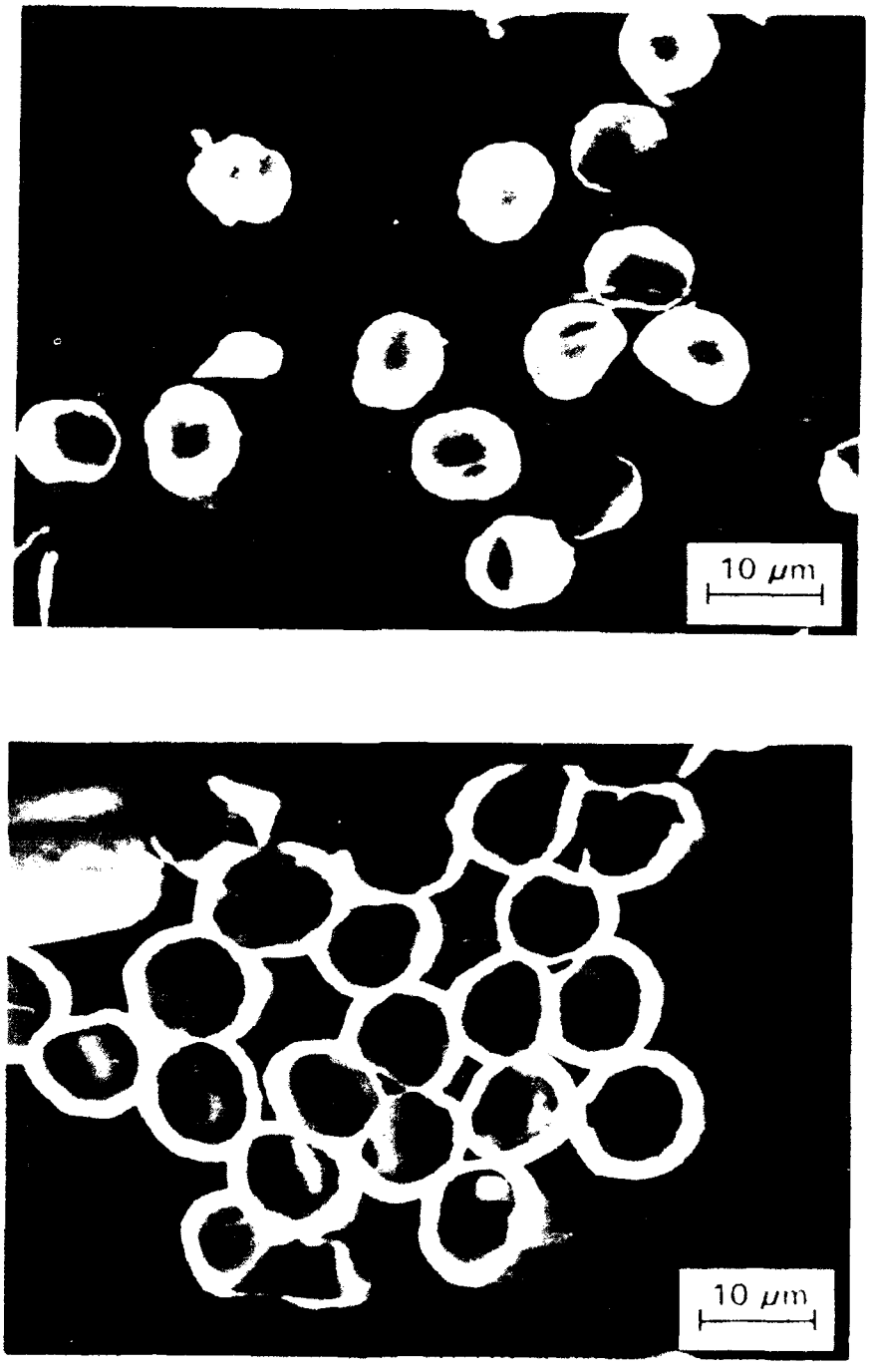


Figure 21. SEM micrographs show the thick and thin coatings deposited during the statistical processing study. For the thick coating, extensive fiber agglomeration was present.

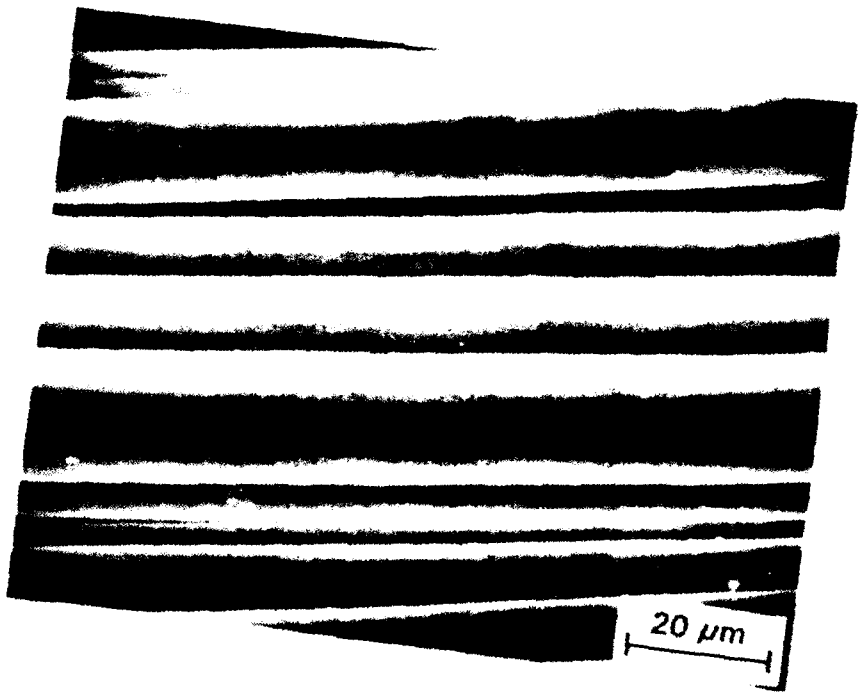


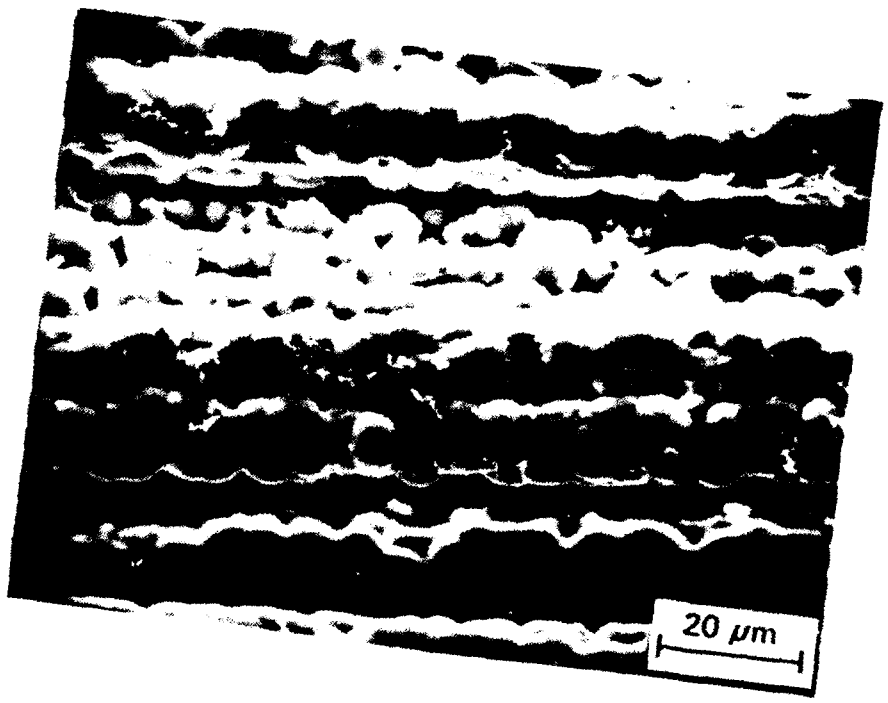


Figure 22. Smooth and rough surface morphology was observed for the runs completed in the study. Smooth surfaces are desired for high strength.

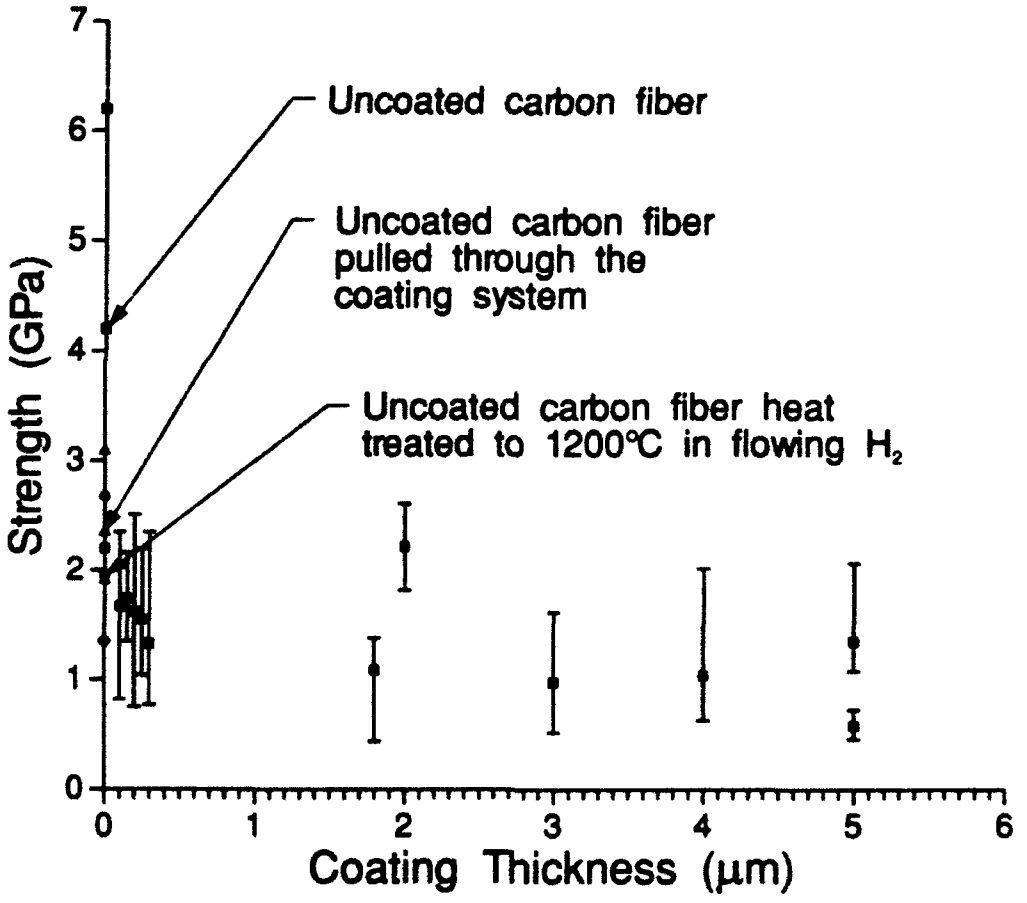


Figure 23. Tensile strength versus coating thickness for SiC coated carbon filaments. The average and data ranges are presented on the figure.

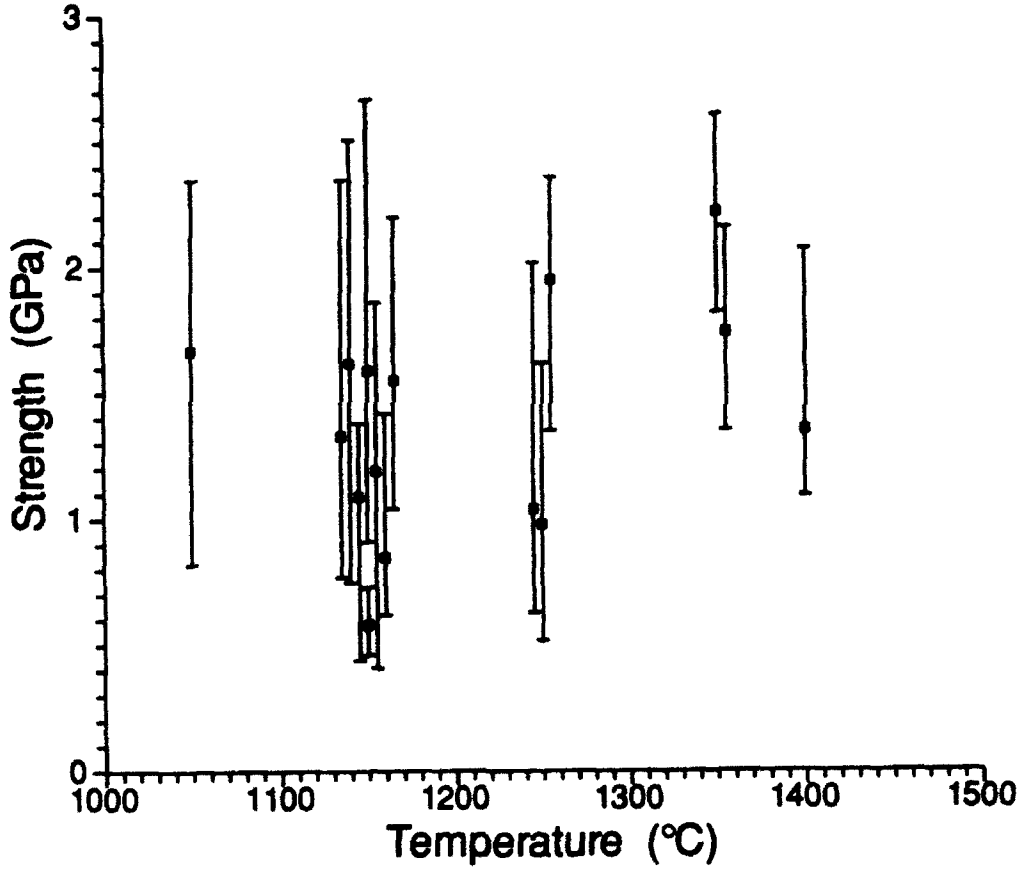


Figure 24. Tensile strength versus deposition temperature for SiC coated carbon fibers; the average and data ranges are shown.

negative influence on the weight gain. Figure 25 is a plot of the weight contour lines (weight of a 15.2 cm fiber) as a function of temperature and MTS flow rate at a fixed value of hydrogen flow rate. All three process variables influence the fiber weight. Weight gain, if desired, can be obtained by subtracting the weight (29 mg) of the uncoated fiber. No correlation was found between the processing variables and strength of the monofilaments. Percent agglomeration was strongly correlated with temperature and MTS flow rate. Figure 26 shows agglomeration contour lines as a function of temperature and MTS flow rate at two $H_2$ flow rates (2.5 and 3.5 $\ell$/min). The strong influences of temperature and MTS flow rate are apparent. In addition, as hydrogen flow rate was increased, the agglomeration decreased (only 81% confidence level).

The box study can be summarized as follows. The amount of coating deposited per unit time increased strongly with increases in the reactor temperature and MTS flow rate but decreased as the hydrogen flow rate was increased. The surface roughness of the coating decreased with increasing hydrogen flow rate. Fiber agglomeration increased with increasing temperature and MTS flow rate; the same factors that had the largest influence on the amount of coating deposited. In fact, a correlation between agglomeration and coating thickness was apparent in the box study as well as for other studies conducted in this program. While strength is likely influenced by the processing variables the scatter in the strength data precluded determining these effects quantitatively.

The box study suggested (81% confidence as shown in Appendix C) that increasing the hydrogen flow rate would decrease the amount of fiber agglomeration. In addition, higher hydrogen flow rates were predicted to give fiber coatings with smoother surfaces. Therefore, a study was performed where the hydrogen flow rate was investigated further.

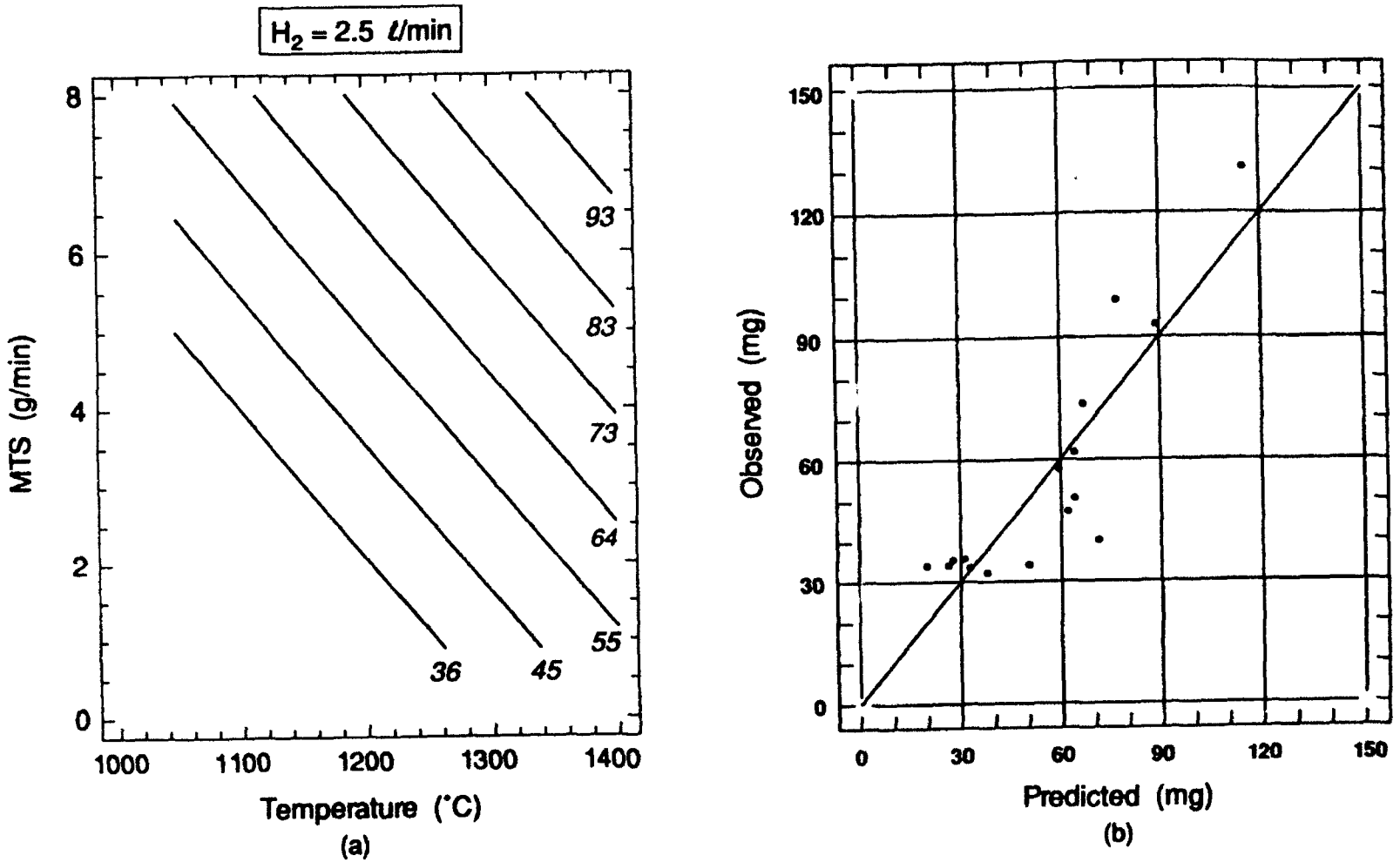


Figure 25. Results of statistical analysis of the weight of a 15.2 cm long coated fiber. A multiple regression model limited to linear terms for temperature, silane flow rate, and hydrogen flow rate was used to predict the fiber weight. (a) Predicted contour lines show the strong effect of MTS flow rate and temperature on fiber weight for a constant $H_2$ flow rate of 2.5 ℓ/min. (b) Plot of observed vs. predicted fiber weight shows good agreement.

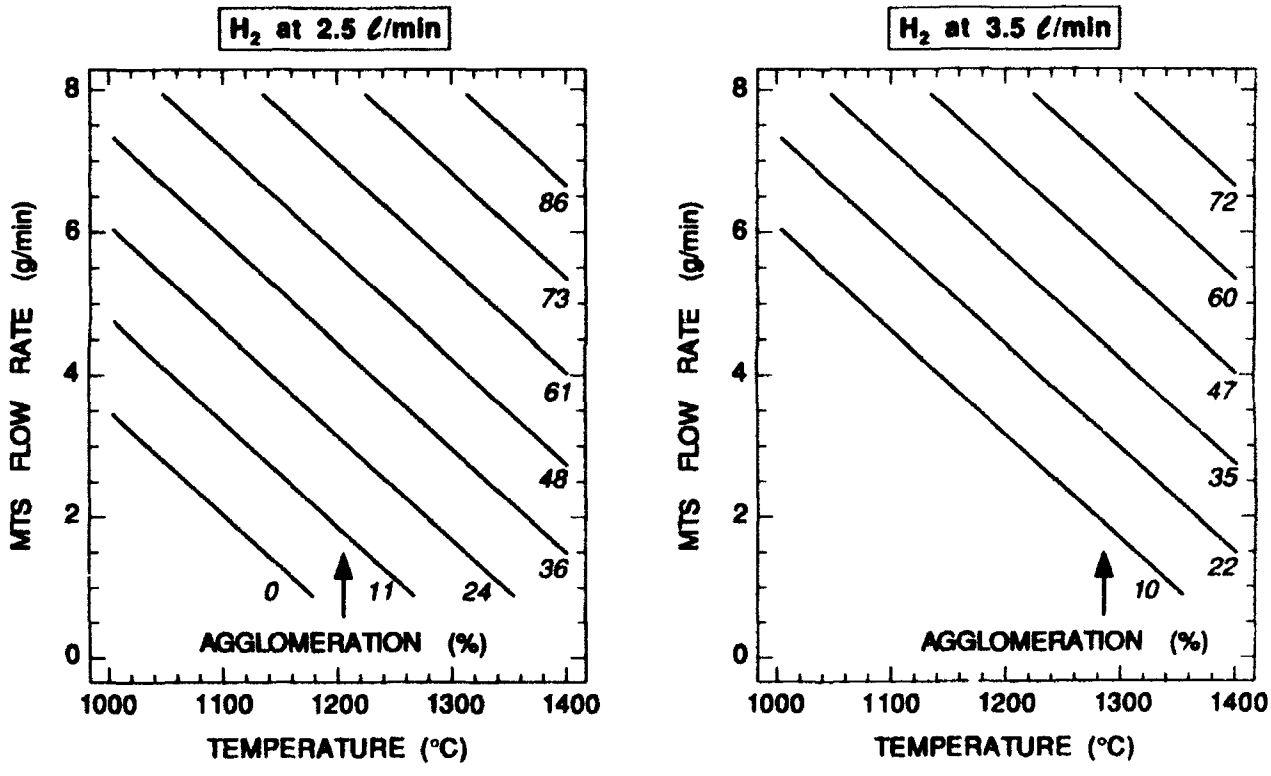


Figure 26. Agglomeration contour lines as a function of the deposition temperature and MTS flow rate for two fixed hydrogen flow rates shows the strong influence of MTS flow rate and temperature on agglomeration and the smaller influence of hydrogen flow rate.

Table 5. Processing-property correlations revealed by the statistical analysis of the box study.

| DEPENDENT VARIABLE | CORRELATING INDEPENDENT VARIABLE | | |
|---|---|---|---|
| | Variable | Significance Level (%) | Effect |
| Strength | None | | |
| Weight Gain<br>$R^2 = 0.79$ | Temperature<br>MTS Flow Rate | >99<br>>99 | +<br>+ |
| Surface Roughness<br>$R^2 = 0.60$ | Hydrogen Flow Rate | 98 | - |
| Agglomeration<br>$R^2 = 0.71$ | Temperature<br>MTS Flow Rate | 97<br>>99 | +<br>+ |

5-3. $H_2$/MTS Ratio Study

In this study, the $H_2$ flow rate was varied from 2.5 to 7 $\ell$/min and the MTS flow rate was varied from 3 to 7 g/min. The results confirmed that higher $H_2$ flow decreased agglomeration due to decreased MTS concentration in the gas stream. However, the higher $H_2$ flow led to the deposition of thinner coatings (< 1 $\mu$m). The results prove that the MTS concentration had a significant effect on agglomeration. The optimal SiC coatings were deposited at 4 $\ell$/min $H_2$ and 5 g/min of MTS. This condition formed a high strength, uniform coating of 2.0 $\mu$m thickness with very little agglomeration (Figure 27).

5-4. Pressure Study

A final processing study was completed which determined the effect of pressure on coating thickness. For the pressure study the temperature, hydrogen flow rate, and MTS flow rate were held constant at (1250°C, 4 $\ell$/min $H_2$, and 7 g/min MTS, respectively). The pressure was increased from 150 to 200 torr. Figure 28 shows the extensive variation of coating

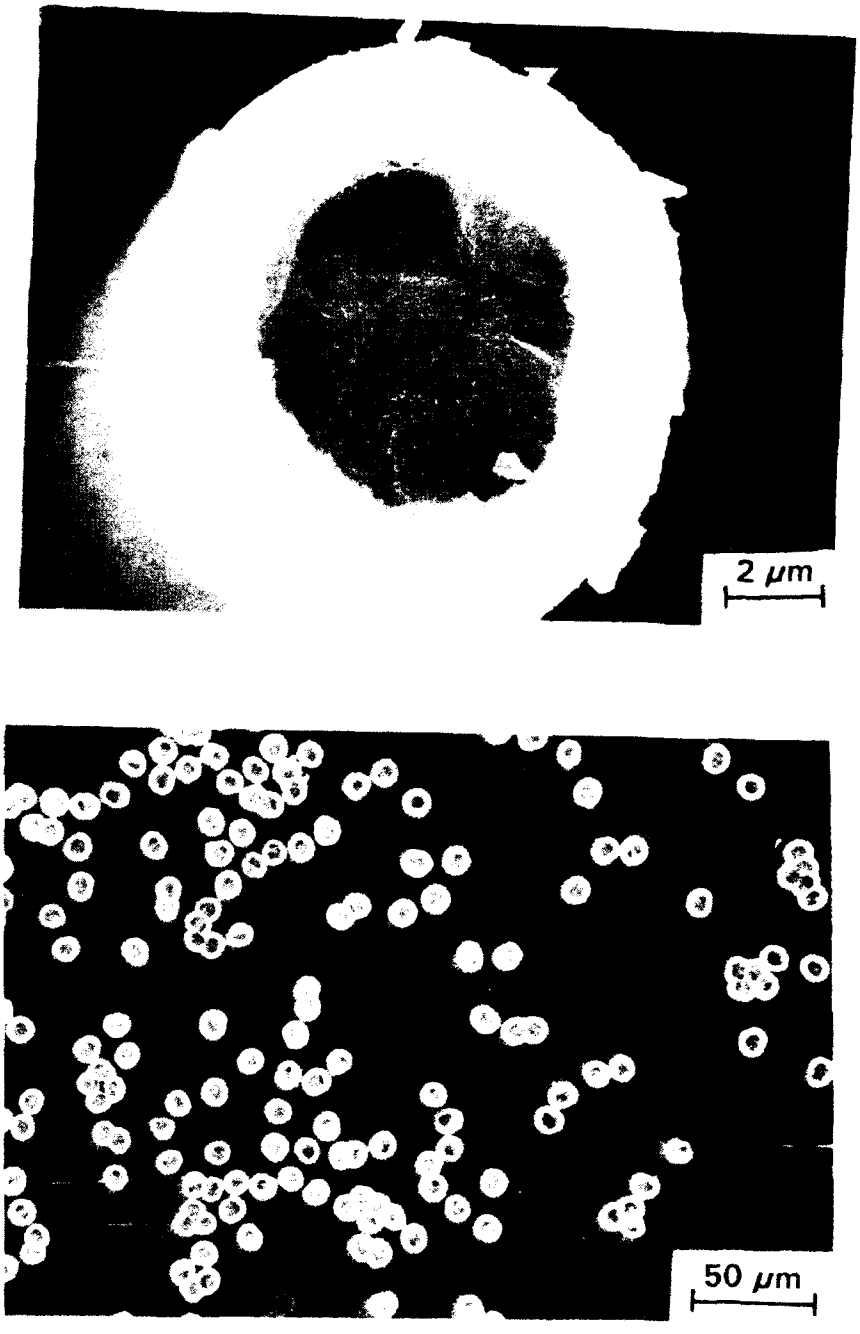


Figure 27. A uniform 2.0 $\mu$m thick coating was deposited using 4 $\ell$/min $H_2$ and 5 g/min MTS flow rates. Very little fiber agglomeration was observed for these conditions.

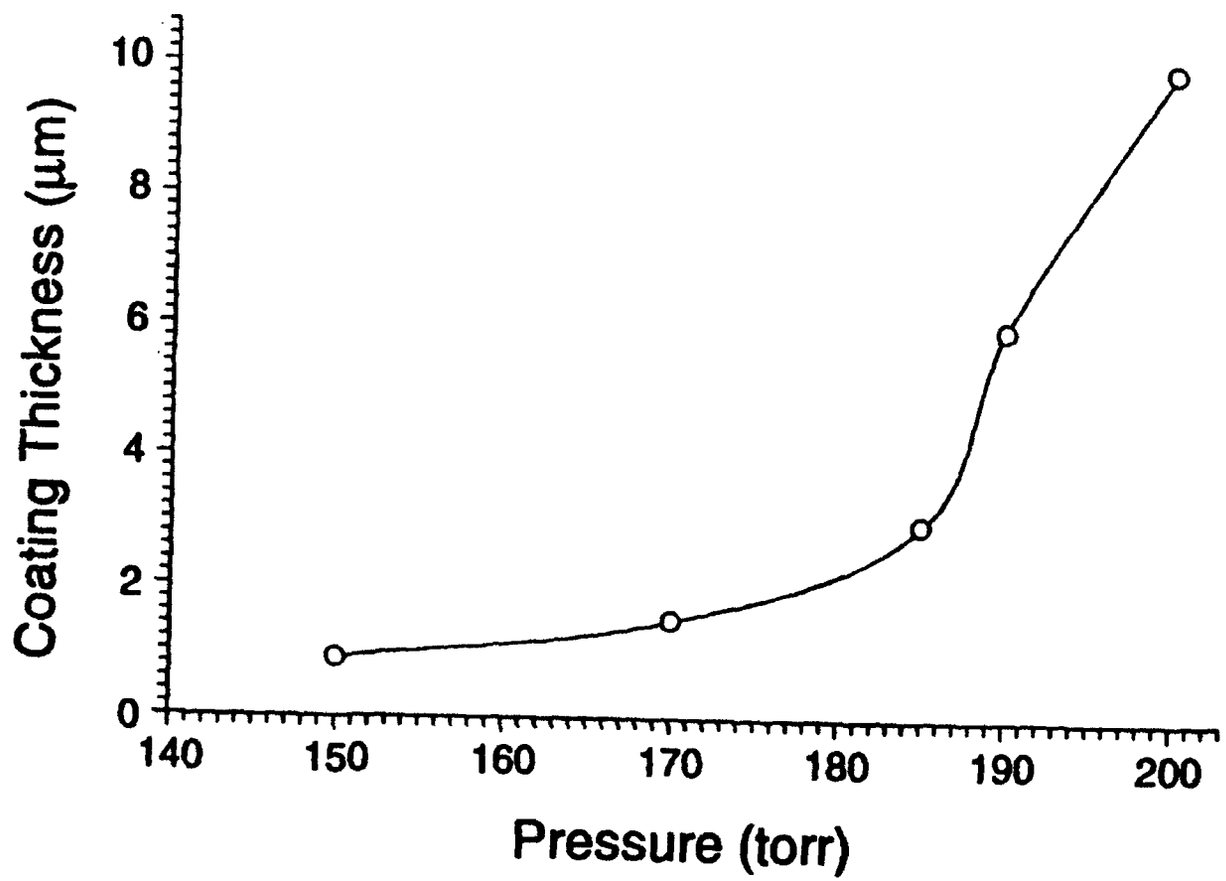


Figure 28. SiC coating thickness versus pressure indicates the wide range of deposition over a fairly narrow processing range.

thickness with pressure. With the conclusion of this study, the deposition process was defined as 1250°C, 4 $\ell$/min $H_2$, 7 g/min MTS, and a pressure approaching 200 torr. The desired coating thickness may be achieved by selection of an appropriate fiber pull speed. As described later, with the more effective fiber spreading techniques developed near the end of this program uniform 5 $\mu$m thick coatings and even higher deposition rates can be obtained at even higher pressures, e.g. 1 atm.

## 6. FIBER SPREADING TECHNIQUES

The study of fiber tow spreading techniques was emphasized following our processing study because fiber tow agglomeration was evident whenever the coating thickness increased to over 1 $\mu$m. Several mechanical spreading techniques, which will be reviewed next, failed to adequately prevent fiber agglomeration or damaged the fiber during processing. The use of more novel spreading devices, including pneumatic and electromagnetic spreading, was pursued later in the project.

### 6-1. Cyclic Tension

The continuous fiber coating system was equipped with a mechanical device that periodically applied and released tension on the fiber tow. This device was controlled by a motor attached to the supply spool in the bottom spool enclosure. A thin metal strip was passed across metal rods attached to a plate which was rotated in the opposite direction of the fiber spool. Adjusting the tension was accomplished by changing the length of the metal strip, or by changing the material used; hardened stainless steel, bronze, teflon, rubber, and plastic were used as the strip material. The resulting action was that the fiber vibrated at the controlled one second intervals.

The best results were obtained using a combination of a hardened stainless steel strip and a rubber strip. The rubber extended the life of the stainless steel by providing some flexibility of the combined material. The tension device was used in conjunction with all the other mechanical spreading techniques.

### 6-2. Gas Jets and Rollers

The statistical processing study was completed using the cyclic tension device and a stationary roller with gas jets (shown in Figure 18). The combination of these techniques spread

the fiber to a tape geometry and increased the tow diameter to 2.5 times the initial diameter. The use of a gas jet, passed through a narrow slit in the roller, caused the fiber to be spread apart and worked with the cyclic tension device. When the tension was released, the fiber tow was blown away from the roller; as tension was applied, the fiber tow was pulled flat against the roller surface and spread like a tape.

This technique was successful for small coating thicknesses (1 $\mu$m and less). As the coating thickness increased, the fibers tended to agglomerate. Another problem with this technique was that at high coating thicknesses, the fiber tow frequently broke due to the violent spreading action. Attempts at lowering the fiber pull rate to increase the coating thickness were inconclusive.

6-3. Fiber Splitting

Efforts to reduce the number of filaments in the fiber tow were attempted based on the earlier modeling work. Initially, carbon fiber tow vendors were contacted for purchase of a fiber tow with less than 3,000 filaments. The only tows with a smaller number of filaments were the Hercules HMU and Amoco T-300, which had 1,000 filaments--but were available only in sized material. The development of carbon tow with fewer filaments was regarded as uneconomical by the vendors. To circumvent this problem, fiber spreaders were used to split the tow effectively into two bundles of filaments being pulled through the coating furnace.

Figure 29 shows the two fiber splitting devices used in the bottom spool enclosure. Both metal strips and metal rollers were used to split the tow. A series of runs was completed which evaluated the size (metal strip versus 0, 1, and 1.5 cm diameter cylindrical spreaders) versus the coating thickness and tensile strength of the filaments. The results are summarized in Table 6. Coating thicknesses varied primarily because of the deliberate use of different MTS flow rates.

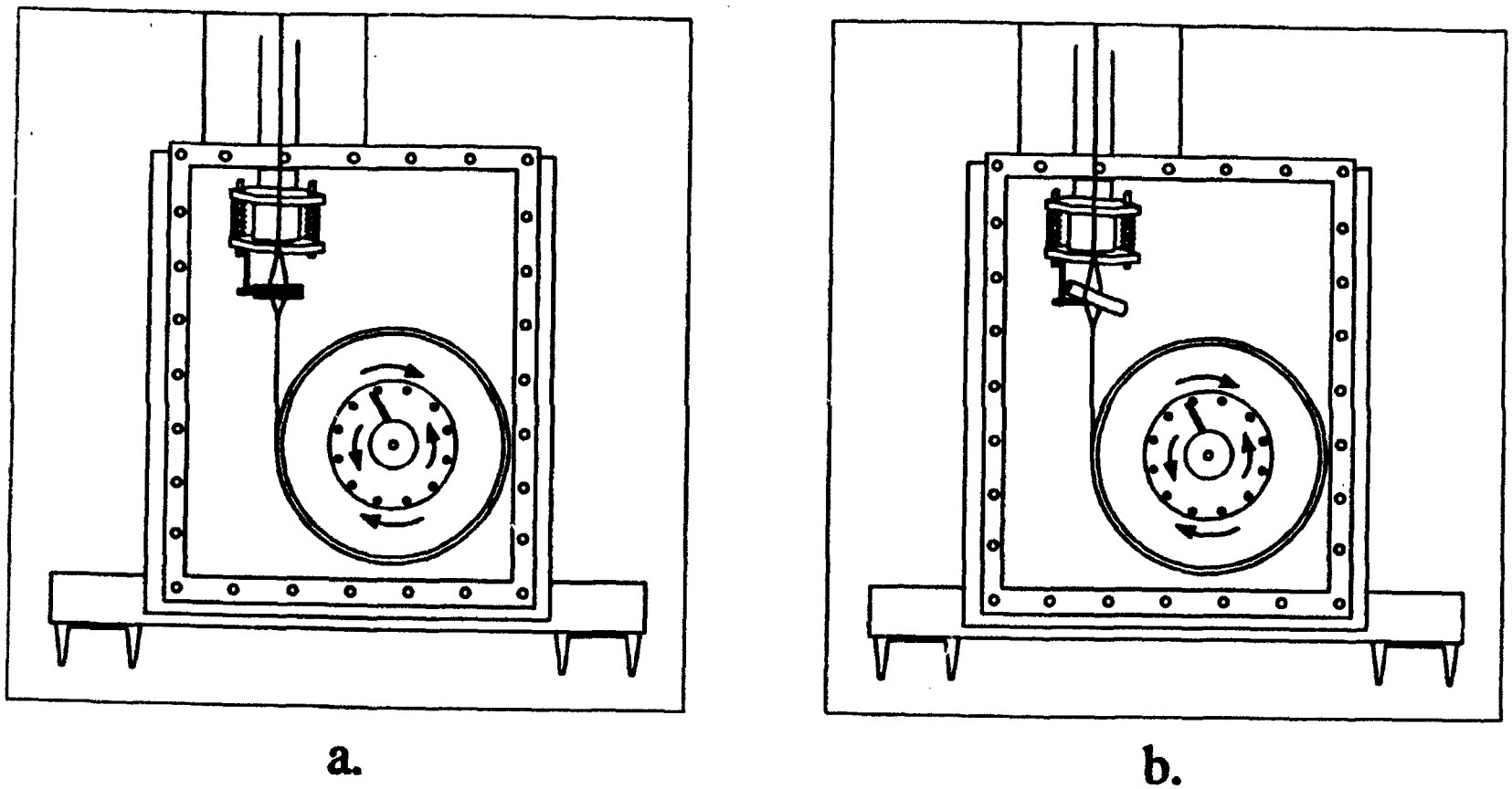


Figure 29. Schematic of the lower supply spool enclosure with both (a) metal strip and (b) cylindrical fiber tow splitters.

Table 6. Summary of fiber splitting study results.

| Run # | Coating Thickness ($\mu$m) | Average Tensile Strength (GPa) | % Fiber Agglomeration |
|---|---|---|---|
| HORIZONTAL METAL STRIP | | | |
| SC107 | 5.65 | 1.16 ± 0.367 | 90 |
| SC119 | 2.70 | 0.73 ± 0.030 | 50 |
| SC127 | 4.75 | 0.63 ± 0.035 | 80 |
| SC128 | 3.5 | 0.76 ± 0.112 | 95 |
| SC142 | 2.0 | 2.41 ± 1.086 | 50 |
| SC143 | 1.5 | 3.78 ± 0.551 | 75 |
| SC153 | 2.25 | 0.60 ± 0.115 | 10 |
| METAL CYLINDER DIAMETER = ½ cm | | | |
| SC130 | 3.5 | 0.88 ± 0.208 | 50 |
| SC132 | 3.5 | 1.76 ± 0.361 | 100 |
| SC133 | 3.25 | 1.19 ± 0.124 | 75 |
| SC151 | 2.25 | 0.96 ± 0.090 | 5 |
| SC152 | 2.25 | 1.29 ± 0.065 | 5 |
| METAL CYLINDER DIAMETER = 1½ cm | | | |
| SC149 | 2.0 | 2.42 ± 0.813 | 5 |
| SC150 | 2.25 | 0.68 ± 0.089 | 5 |
| METAL CYLINDER DIAMETER = 1 cm | | | |
| SC146 | 1.25 | 0.71 ± 0.182 | 5 |
| SC147 | 3.90 | 0.54 ± 0.114 | 5 |
| SC148 | 1.5 | 0.68 ± 0.051 | 5 |

The use of metal strips was preferred; both thick coatings and high tensile strengths were achieved using this technique. The major drawback to this mechanical spreading was that the fiber tended to bunch together where the splitting was accomplished. Long run times were difficult to achieve with the mechanical splitting technique because "fiber balls" often formed.

6-4. Pneumatic Spreading

The pneumatic spreading technique, which was presented by Kim and Gray[53], was used to spread the filaments of the carbon tow. One of the unique features of this technique was that no mechanical force was used with the fiber. A schematic of this technique, which was modified to a cylindrical geometry for the continuous fiber coating furnace, is shown in Figure 30. The operating principle involved using a vacuum pump to provide a high throughput of gas down restricted inlet tubes (points A and B in the figure) and utilized the gas flow to force the filaments apart. This approach successfully spread the fiber tow into a wide tape provided the fiber was not in tension.

The pneumatic spreading device was placed in the bottom supply spool enclosure. In order to achieve minimum fiber tension, the supply spool was rotated at a slightly higher speed than the take-up spool. Also, a gas diffusion ring was attached above the cylinder to both impinge jets of gas onto the fiber tow and to provide the gas necessary to assist in spreading the fiber. Another concern involved maintaining a higher pressure in the lower spool enclosure than the CVD furnace which prevented any diffusion of the reactants into the enclosure.

Initial experiments utilizing this approach appeared to spread the fiber tow to 3 times the initial diameter; a tape geometry was created. A small study which varied the MTS and $H_2$ diluent flow rates was completed. The processing parameters were affected by the large $H_2$ flow rate required to spread the fiber tow in the bottom spool enclosure. The results from this study

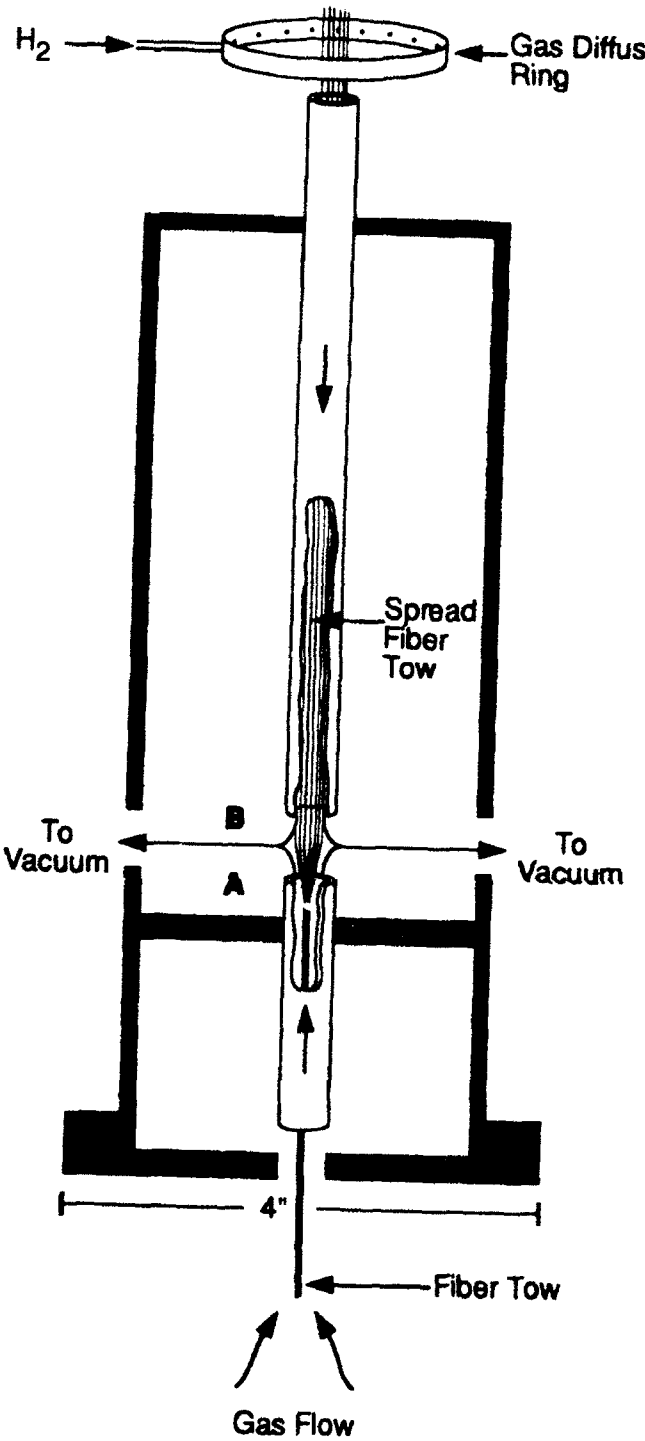


Figure 30. Schematic of the pneumatic induction cylinder used to spread the fiber tow.

were encouraging; thick SiC films (i.e. ~5 $\mu$m) were deposited with a reduced amount of agglomeration (<30 %) than had been previously observed for thick coatings using any of the mechanical spreading techniques.

6-5. Electromagnetic Spreading

A final spreading technique which involved the use of electromagnetic forces on the fiber tow gave the most successful results. This technique was developed by Sheehan et al.[54] at MSNW, Inc. The technique is shown schematically in Figure 31; the spreading involved passing an alternating current through the fiber tow using a 100 watt frequency generator, and surrounding the fiber external to the system with two 500 Gauss permanent horseshoe magnets. The initial work with this spreading technique was exciting due to the fact that the tow was spread to about 2 cm diameter and could be vibrated in a controlled fashion.

The modeling of the spreading of the fiber tow involved solving the wave equation:

$$\delta^2 y/\delta t^2 = c^2\, \delta^2 y/\delta x^2,$$

where $c = (T/\rho)^{0.5}$

$T$ = fiber tension

$\rho$ = linear fiber density

$y$ = transverse displacement, i.e., how wide the fiber tow spreads

$t$ = time

$x$ = axial position

For fiber tow spreading, the solution to this equation for two nodes is:

Frequency = $[T/\rho]^{0.5}/2\ell$ where $\ell$ is the length of tow being spread. A node corresponds to the positions where the fiber tow is not spread. The maximum spreading $y_{max}$, is proportional to the

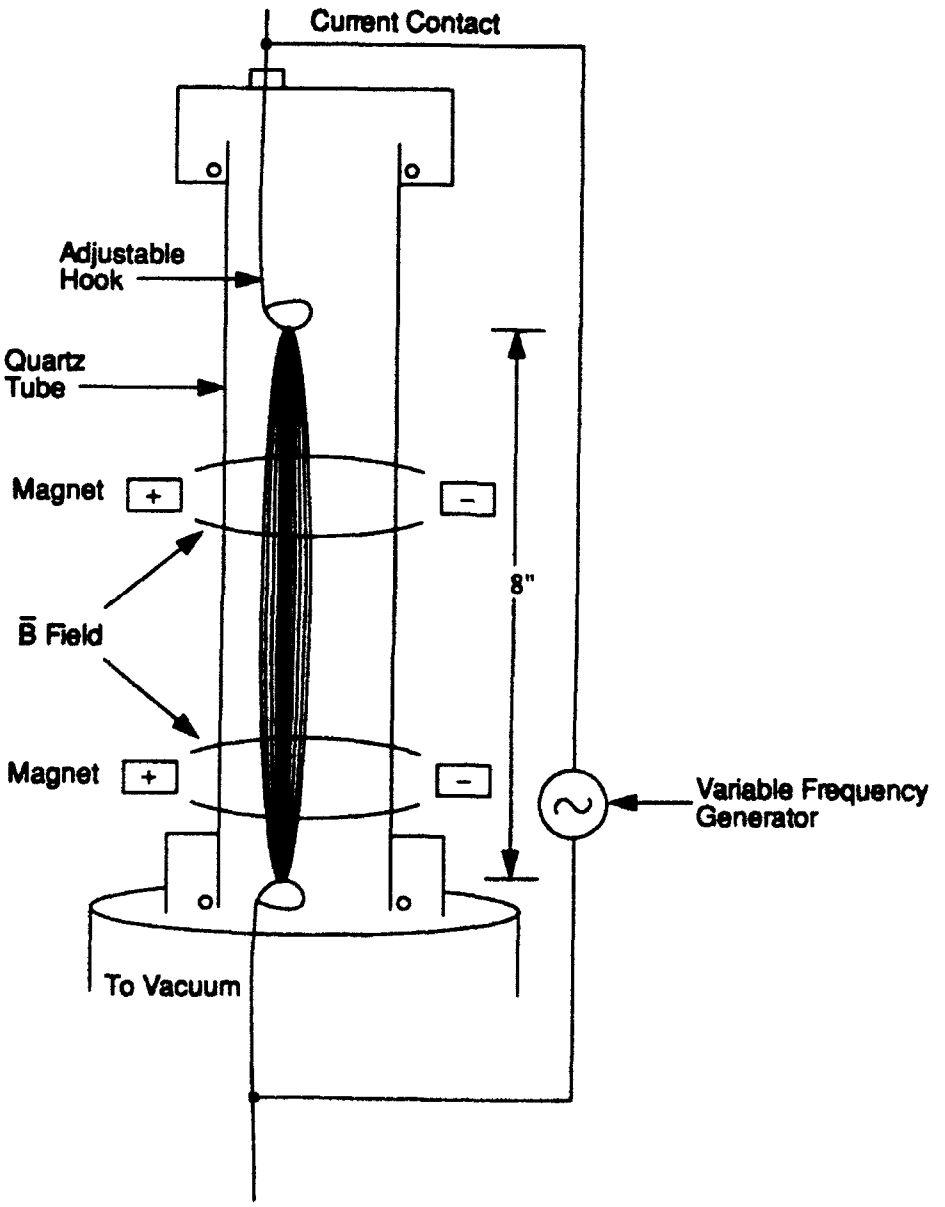


Figure 31. Schematic of the electromagnetic fiber spreading technique.

magnitude of the driving force, which is the cross product of the electrical and magnetic forces, and inversely proportional to the tension in the fiber.

The results from this spreading technique are shown in Figure 32. These static CVD experiments were completed in a small glass tube used to monitor the spreading. The current, which was typically 2-3 Amps, heated the ~25 cm long carbon fiber. Several experiments which studied the effect of tension, pressure, current, and frequency were completed in order to understand the wave relationships to provide maximum spreading in the anti-node position. The preferred operating conditions were determined to be 3 Amps (which was required to adequately heat the fiber) and a frequency of 50 to 100 Hz. Standard 60 Hz power regulated with a Variac worked well. As the voltage (i.e. current) was increased to initiate a run, on some occasions, the tow would move as a unit rather than as individual filaments. This could be observed visually. However, before the desired voltage level was achieved, the tow would invariably spread, i.e., the individual filaments moved separately to form the configuration shown in Figure 32 or a similar configuration having 1 or 2 nodes. Further description of the benefits of this technology in relation to a commercial process is detailed in the following section.

Figure 32. Photograph of the electromagnetic technique in operation shows a zero node state of the fiber tow spread to 2 cm tow diameter.

## 7. CONCEPT FOR SCALE-UP

Throughout the course of this research we constantly kept in mind that the process and CVD fiber coating equipment should be amenable to scale-up necessary for commercial operation. This consideration argues for safe, inexpensive, reliable, easily operated equipment capable of high throughput. The research and development conducted to date offers encouragement. Our thoughts regarding the conceptual design of a commercial CVD system for preparing large quantities of inexpensive SiC fiber tow follow.

The concept is very similar to that used by Textron to fabricate boron monofilament and presumably similar to that used for fabricating SCS-6 SiC monofilament. A simple cold wall continuous CVD system is proposed. The carbon fiber tow substrate would be heated resistively. Electrical connections with the fiber would be accomplished by the use of mercury contacts. The fiber would be spread extensively using the electromagnetic method. By locating the mercury contacts near the ends of the reactor but in a region where the fiber is partially spread the mercury will readily infiltrate the tow to permit good contact with each filament. (Alternatively, pressure plates or metal rollers could be used to provide electrical contact.)

The reaction chamber would be made of glass and have dimensions of about 1 inch diameter by 10 feet long. The reagent stream would enter one end of the reaction chamber and exit the other. It is not anticipated that multiple reagent inlets would be needed. This permits a very simple, inexpensive, reliable reactor design. The use of a cold wall reactor greatly enhances reagent utilization since almost all of the deposition is on the fiber. The recycle of reagents may be possible but considerable development is necessary before this can be asserted with any confidence.

It is anticipated, based on the following argument that very high coating rates could be achieved. First, as we have demonstrated, the electromagnetic spreading technique causes extensive spreading of the fiber tow. This is significant since previously there was the necessity to use low total gas pressure in order to assist infiltration of the reagent(s) into the fiber tow in order to obtain coating uniformity. Low pressures almost invariably reduce the rate of coating deposition. With extensive spreading of the fiber high pressures (i.e., 1 atmosphere) can be used without sacrificing coating uniformity. Also, since the electromagnetically spread fiber is constantly in motion there is little likelihood of one filament sticking to another. This, and the use of a cold wall reactor, prevents fibers from sticking to the wall of the reactor and thus accumulation of fiber debris is minimized or eliminated.

In summary, with the proposed coating system it should be possible to rapidly fabricate high quality SiC fiber tows. The fact that SiC monofilaments having coating thicknesses several tens of microns have been similarly prepared by others at fiber pull speeds of several feet per minute provides further confidence in the conceptualized process. Our success in development of the electromagnetic fiber spreading technique encourages us that fabrication of high quality SiC fiber tows by the CVD technique is indeed a realistic goal.

## 8. CONCLUSIONS

Results from this effort indicate that the continuous deposition of SiC onto small diameter carbon fiber tows is a feasible process for fabricating strong SiC fibers for use in ceramic and metal matrix composites provided that the fiber tow is spread effectively during deposition. Uniform coatings with fiber tensile strengths in excess of 2 GPa have been achieved. Extensive modeling efforts were performed which led to an increased understanding of the fiber coating process and final fiber/coating stress states which assisted in selection of the carbon fiber substrate. The process modeling also can be used to assist in modifying the process to a commercial scale.

Experimental work was completed in two major areas; understanding the deposition of SiC onto fibers and evaluating various fiber spreading techniques. The deposition of SiC was studied using a statistically designed study; processing-property correlations were determined using multiple regression analysis. The use of several mechanical spreading techniques was evaluated; the results were inconclusive due to a wide variation of tensile strengths, and the judgement that the fibers were agglomerated an unacceptable amount. The final fiber spreading techniques evaluated were more encouraging since they did not rely on any mechanical device; both pneumatic and electromagnetic spreading are techniques which solve the agglomeration problem without damage to the fiber tow.


## ACKNOWLEDGMENTS

We would like to thank Dr. Allan Katz for funding this work and for helpful technical discussions. He correctly suggested that development of a fiber spreading technique was critical to success of this project. Dr. Paul Jero is also acknowledged for his technical input to this program and his thorough, constructive review of this report.

## 9. REFERENCES


1. C.F. Powell, I.E. Campbell, and B.W. Conser, "Vapor Plating," pp. 9-11, John Wiley and Sons, NY, 1955.

2. P.H. Higgs, R.L. Finicle, R.J. Bobka, E.J. Seldin, and K.J. Zeitsch, "Research and Development on Advanced Graphite Materials," Report No. WADD TR 61-72, May 1964.

3. E. Saunders, Martin Weinstein, and A.I. Mlavsky, "Radiant Energy Reactor Technique for the Deposition of SiC onto Quartz Filaments," pp. 217-27 in Proceedings of the Conference on Chemical Vapor Deposition of Refractory Metals, Alloys, and Compounds, American Nuclear Society, Hinsdale, IL, 1967.

4. Lloyd E. Line, Jr., and U.V. Henderson, Jr., "Boron Filament and Other Reinforcements Produced by Chemical Vapor Plating," pp. 201-36 in Handbook of Fiberglass and Advanced Plastics Composites, ed. George Lubin, Van Nostrand Reinhold Co., NY, 1969.

5. H.E. DeBolt, V.J. Krukokonis, R.M. Neff, F.E. Wawner, SAMPE, "Chemical Vapor Deposition of Boron on a Carbon Monofilament Substrate," Materials Review for '72, Vol. 17, pp. II-B-Two-1 - II-B-Two-10.

6. E. Fitzer, D. Kehr, and M. Sahebkar, "CVD-SiC on Carbon Fibres," pp. 33-41 in Proceedings of the Third International Conference on Silicon Carbide, Miami Beach, FL. 1973.

7. H.E. DeBolt, V.J. Krukonis, and F.E. Wawner, Jr., "High Strength, High Modulus Silicon Carbide Filament via Chemical Vapor Deposition," ibid., pp. 168-75.

8. W.J. Heffernan, I. Ahmad, R.W. Haskell, "A Continuous CVD Process for Coating Filaments with Tantalum Carbide," pp. 498-508 in Proceedings of the Fourth International Conference on Chemical Vapor Deposition, The Electrochemical Society, Inc., Princeton, NJ, 1973.

9. L. Aggour, E. Fitzer, E. Ignotowitz, and M. Sahebkar, "Chemical Vapour Deposition of Pyro-Carbon, SiC, TiC, TiN, Si and Ta on Different Types of Carbon Fibers," Carbon 12, 358-62 (1974).

10. R. Warren and M. Carlsson, "TiC- and TiN-Coated Carbon Fibres," pp. 623-33 in Proceedings of the Fifth International Conference on Chemical Vapor Deposition, The Electrochemical Society, Inc., Princeton, NJ, 1975.

11. E. Fitzer, D. Kehr, D. Morin, and M. Sahebkar, "Deposition of Silicon Carbide on Carbon Monofilaments," ibid., pp. 589-99.

12. M.J. Hakim, "Chemical Vapour Deposition of Hafnium Nitride and Hafnium Carbide on Tungsten Wires," ibid., pp. 634-49.

13. V.G. Samoilenko and L.N. Pereselentseva, "Deposition of Zirconium Carbide Coatings Acting as Diffusion Barriers in Composites Consisting of a Metallic Matrix and Refractory Metal Fibers," Soviet Powder Met. and Metal Ceramics, Vol. 14, pp. 725-28, 1975.

14. R.J. Imprescia, L.S. Levinson, R.D. Reiswig, Terry C. Wallace, and J.M. Williams, "Carbide Coated Fibers in Graphite-Aluminum Composites," Los Alamos Scientific Laboratory, LA-6181-PR, July 1976.

15. J.A. Cornie, "Characterization, Shaping, and Joining of SiC/Superalloy Sheet for Exhaust System Components," Electric Corp., Report No. NASA CR-135301, July, 1977.

16. V. Krukonis, I. Chemical Vapor Deposition of Boron Filament, pp. 517-40 in Boron and Refractory Borides, Springer-Verlag, New York, 1977.

17. M.J. Hakim, Chemical Vapor Deposition, U.S. Patent No. 4,107,352, August 15, 1978.

18. L.R. Newkirk, R.E. Riley, H. Sheinberg, F.A. Valencia, and T.C. Wallace, "Preparation of Unidirectional Fiber Reinforced Tantalum Carbide Composites," pp. 488-98 in Proceedings of the Seventh International Conference on Chemical Vapor Deposition, The Electrochemical Society, Inc., Princeton, NJ, 1979.

19. F.S. Galasso, R.D. Veltri, and D.A. Scola, Study of High Resistance Inorganic Coatings on Graphite Fibers, United Technologies Research Center, East Hartford, CT, NASA-CR-159078, June, 1979.

20. K. Brennfleck, M. Dietrich, E. Fitzer, and D. Kehr, "Chemical Vapor Deposition of Superconducting Niobium Carbonitride Films on Carbon Fibers," pp. 300-14 in Proceedings on the Seventh International Conference on Chemical Vapor Deposition, The Electrochemical Society, Inc., Princeton, NJ, 1979.

21. R.J. Suplinskas and T.W. Henge, "A Study of the Deposition of Carbide Coatings on Graphite Fibers," Avco Specialty Materials Division, Lowell, Massachusetts, NASA Contractor Report 159133, September, 1979.

22. John B. MacChesney, "Materials and Processes for Preform Fabrication-Modified Chemical Vapor Deposition and Plasma Chemical Vapor Deposition," Proceedings of the IEEE, 68 [10] 1181-84 (1980).

23. F. Schmaderer, G. Wahl, C.H. Dustmann, and M. Dietrich, "CVD-$NbC_{1-y}N_y$-Carbon Fiber Superconductors," pp. 148-55 in Proceedings of the Fourth European Conference

on Chemical Vapor Deposition, Philips Centre for Manufacturing Technology, Eindhoven, The Netherlands, 1983.

24. E. Wilfing, F. Holub, and E. Horl, "Chemical Vapor Deposition of $Nb_3Sn$ in a Fluidized Bed," ibid., pp. 156-63.

25. K. Brennfleck and E. Fitzer, "SiC-Coatings as Protective Layers for Carbon Fibers and Adhesion Promoters for Superconducting Niobium Carbonitride," ibid., pp. 370-75.

26. K. Brennfleck, E. Fitzer, G. Schoch, and M. Dietrich, "CVD of SiC-Interlayers and Their Interaction with Carbon Fibers and with Multi-Layered NbN Coatings," pp. 649-62 in Proceedings of the Ninth International Conference on Chemical Vapor Deposition, The Electrochemical Society, Inc., Pennington, NJ, 1984.

27. F. Schmaderer, G. Wahl, M. Dietrich, and C.H. Dustmann, "Preparation of Al-Stabilized Superconducting $NbC_{1-y}N_y$-Carbon Fibers," ibid., pp. 663-72.

28. Akio Shindo, "Chemical Property of Carbon Fiber Surface and Interfacial Compatibility of Composites," pp. 93-100 in Composite Interfaces, Proceedings of the First International Conference on Composite Interfaces, North Holland, NY, 1986.

29. Kuniaki Honjo and Akio Shindo, "Interfacial Behavior of Aluminum Matrix Composites Reinforced with Ceramics-Coated Carbon Fibers," ibid., pp. 101-107.

30. Barry Bender, Damian Shadwell, Charles Bulik, Louis Incorvati, and David Lewis III, "Effect of Fiber Coatings and Composite Processing on Properties of Zirconia-Based Matrix SiC Fiber Composites," Am. Ceram. Soc. Bull. 65 [2] 363-69 (1986).

31. Joel P. Clark and Merton C. Flemings, "Advanced Materials and the Economy," Scientific American 255 [4] 51-58, October 1986.

32. D.K. Nath, "A Method for Strengthening Silica Fiber," J. Am. Ceram. Soc. 65 [5] 752 (1986).

33. Roy W. Rice, BN Coating of Ceramic Fibers for Ceramic Fiber Composites, U.S. Patent No. 4,642,271, February 10, 1987.

34. E. Fitzer, "Ceramic and Coated Carbon Fibers for High Temperature Ceramics," pp. 9-52 in Whisker- and Fiber-Toughened Ceramics, ASM International, 1988.

35. W.J. Lackey and T.L. Starr, "Fabrication of Fiber-Reinforced Ceramic Composites by Chemical Vapor Infiltration: Processing, Structure and Properties," pp. 397-450 in Fiber Reinforced Ceramics, ed. K.S. Mazdiyasni, Noyes Publications, Park Ridge NJ (1990).

36. W.J. Lackey, W.B Carter, John A. Hanigofsky, D.N. Hill, E. Kent Barefield, Galina Neumeier, David F. O'Brien, Michael J. Shapiro, John R. Thompson, Andrew J. Green,

and Thomas S. Moss, III, "Rapid Chemical Vapor Deposition of Superconducting $YBa_2Cu_3O_X$," Appl. Phys. Lett. 56 [12] 1175-77, March 19, 1990.

37. W.J. Lackey, J.A. Hanigofsky, M.J. Shapiro, W.B. Carter, D.N. Hill, E.K. Barefield, E.A. Judson, D.F. O'Brien, Y.S. Chung, and T.S. Moss, "Preparation of Superconducting Wire by Deposition of $YBa_2Cu_3O_X$ onto Fibers," pp. 195-210 in Eleventh International Conference on Chemical Vapor Deposition, Seattle, WA, October 14-19, 1990, The Electrochemical Society, Pennington, NJ.

38. T.M. Besmann, Processing Science for Chemical Vapor Infiltration, Industry/Government Briefing, Oak Ridge National Laboratory, Oak Ridge, TN, November 9, 1990.

39. W.J. Lackey, John A. Hanigofsky, Michael K. Groves, and Joseph A. Heaney, "Continuous Fiber Coating System," pp. 1048-63 in Proceedings of the 15th Annual Conference on Composites and Advanced Ceramics, Cocoa Beach, FL, The American Ceramic Society, January 13-16, 1991.

40. W.J. Lackey et al., "Ceramic Coatings for Heat Engine Materials-Status and Future Needs, ORNL/TM-8959, Oak Ridge National Laboratory, Oak Ridge, Tennessee.

41. T. Narushima, T. Goto, and T. Hirai, "High-Temperature Passive Oxidation of Chemically Vapor Deposited Silicon Carbide," J. Am. Ceram. Soc., 72 [8] 1386-90 (1989).

42. G.S. Corman, "Creep of Oxide Single Crystals," GE Corporate Research and Development Center, WRDC-TR-90-4059, Materials Laboratory, WRDC, Wright-Patterson AFB, OH, August 1990.

43. Eriksson, G., "Thermodynamic Studies of High Temperature Equilibria," Chemica Scripta, 8, (1974).

44. D.R. Lide, Jr., (ed.), Janaf Thermochemical Tables, 3rd edn., Vols. I and II, American Chemical Society and American Institute of Physics for National Bureau of Standards (US), 1985.

45. I. Barin, O. Knacke and O. Kubaschewski, Thermochemical Properties of Inorganic Substances: Supplement, Springer, Berlin, 1977.

46. Satterfield, C.N. and Sherwood, T.K., "The Role of Diffusion in Catalysis, Chapter 3, Addison-Wesley Publishing Co., Inc., Reading, MA (1963).

47. Starr, T.L., "Modeling of Forced Flow/Thermal Gradient CVI," Proceedings on International Conference on Whisker- and Fiber Toughened Ceramics," pp. 1-6, June 7-9, 1988, Oak Ridge, TN.

48. Starr, T.L., "Model for Rapid CVI of Ceramic Composites," pp. 1147-55 in Proceedings of the 10th Int. Conf. on CVD, October 1987, Edited by G.W. Cullen, The Electro. Chem. Soc., Pennington, NJ, Vol. 87-88.

49. Besmann, T.M., Sheldon, B.W., and Kaster, M.D., "Temperature and Concentration Dependence of SiC Deposition on Nicalon Fibers," Surface and Coatings Technology, 43/44, 167-175 (1990).

50. J.A. Hanigofsky, "Modeling of the Chemical Vapor Deposition of $YBa_2Cu_3O_x$, $TiB_2$, and SiC Thin Films Onto Continuous Ceramic Tows," Ph.D. Dissertation, School of Materials Engineering, Georgia Institute of Technology, Atlanta, GA, September, 1992.

51. C.H. Hsueh, P.F. Becher, and W.J. Lackey, "Thermal and Mechanical Induced Stresses in Superconducting $YBa_2Cu_3O_x$ Coatings on Fibers," J. Appl. Phys. 70(3), 1337-41, August 1, 1991.

52. M.G. Ellenburg, J.A. Hanigofsky, and W.J. Lackey, "Thermal Stress Analysis for Coated Fibers," submitted to J. Mater. Res., April, 1993.

53. C. Kim and R.A. Gray, "Pneumatic Induction Fiber Spreader with Lateral Venturi Restrictors," Dept. of the Navy, Office of the Chief of Naval Research, patent application, Serial Number 131,684, 1987.

54. J.E. Sheehan, J.T. Porter, C.H. Meyers, R.J. Price, and R. Bacon, "Coated Carbon Fiber Development for Oxidation Protection of Carbon-Carbon Composites," Interim Progress Report No. 10, Contract No. F33615-88-C-5449, MSNW, Inc., San Marcos. CA 1990.

# APPENDIX A

## Mathematical Development of Process Model

# APPENDIX A

## Mathematical Development of Process Model

This appendix describes the theoretical derivation for the solution to the partial differential equation which relates the competition between the reaction rate and diffusion steps for a chemical process. A brief description of the Chapman-Enskog pseudo-binary diffusion coefficient calculation is also presented.

The solution procedure is similar to the catalysis work presented by Satterfield and Sherwood[46]; however, the catalysis work they presented is for spherical coordinates. The fiber processing problem utilizes cylindrical coordinates, which complicates the analysis. Instead of a theoretical solution a series solution is required. For the zero order reaction rate (Rate = $K_v$) the differential equation can be written as:

$$\frac{d^2c}{dr^2} + \frac{1}{r}\frac{dc}{dr} = \frac{K_v}{D}$$

multiplying through by $r^2$ gives:

$$r^2\frac{d^2c}{dr^2} + r\frac{dc}{dr} = \frac{K_v}{D}r^2$$

A complete solution of the equation consists of a solution of the homogeneous equation and the particular solution.

The homogeneous equation is:

$$r^2\frac{d^2c}{dr^2} + r\frac{dc}{dr} = 0$$

This second order homogenous ordinary differential equation has the form of a Cauchy-Euler Equation, which has the general solution:

$$C_h = A + B\ln r \quad \text{where } A, B \text{ are constants}$$

The solution to the homogeneous part can be verified by inserting the solution into the differential equation, e.g.:

$$-\frac{dc}{dr} = \frac{1}{r} \qquad \frac{d^2c}{dr^2} = -\frac{1}{r^2}$$

$$-\frac{1}{r^2}r^2 + r\frac{1}{r} = 1-1 = 0$$

$$C_h = A + B\ln r$$

Using the first boundary condition:

$$C \text{ finite} \atop @\ r = 0 \rightarrow B = 0$$

$$C_h = A \qquad C = C_h + \text{particular solution}$$

The particular solution is solved as follows:

Choosing a solution for the equation, where B is a constant

$C_p = Br^2$. Plugging this expression into the differential equation:

$$\frac{dC_p}{dr} = 2Br$$

$$\frac{d^2C_p}{dr^2} = 2B$$

Setting the two sides of the equation equal:

$$r^2 \cdot 2B + r \cdot 2Br = \frac{K_v}{D} r^2$$

$$4Br^2 = \frac{K_v}{D} r^2$$

$B = \frac{K_v}{4D} r^2$, which is the value for the constant $B$:

$$C_p = \frac{K_v}{4D} r^2$$

$c = c_h + c_p$ defines the complete solution:

$$= A + \frac{K_v}{4D} r^2$$

The value for A can be determined using the following boundary condition:

$$\left.\frac{dc}{dr}\right|_{r=0} = \left.\frac{K_v}{2D} r\right|_{r=0} = 0$$

$$c|_{r=R} = C_R = A + \frac{K_v}{4D} R^2$$

$$A = C_R - \frac{K_v}{4D} R^2$$

$$\frac{dc}{dr}|_{r=0} = \frac{K_v}{2D} r|_{r=0} = 0$$

$$C|_{r=R} = C_R = A + \frac{K_v}{4D} R^2$$

$$A = C_R - \frac{K_v}{4D} R^2$$

The solution for the zero order reaction rate for the differential equation is:

$$C(r) = C_R - \frac{K_v}{4D} (R^2 - r^2)$$

or, in a more convenient form:

$$\frac{C}{C_R} = 1 - \frac{K_v}{4C_R D}(R^2 - r^2)$$

The 1st order reaction expression, Rate = $K_v C$ results in the ordinary differential equation:

$$\frac{d^2c}{dr^2} + \frac{1}{r}\frac{dc}{dr} = \frac{K_v}{D}C$$

which can be rewritten as:

$$r^2\frac{d^2c}{dr^2} + r\frac{dc}{dr} - \frac{K_v}{D}r^2C = 0$$

Defining a constant W for convenience:

$$W = \sqrt{\frac{K_v}{D}}r$$

so:

$$W^2 = \frac{K_v}{D}r^2$$

The differential equation can be rewritten in terms of W, which is presented in several steps:

$$\frac{dc}{dr} = \frac{dc}{dw}\frac{dw}{dr} = \sqrt{\frac{K_v}{D}}\frac{dc}{dw}$$

$$r\frac{dc}{dr} = \frac{1}{\sqrt{\frac{K_v}{D}}} W\sqrt{\frac{K_v}{D}}\frac{dc}{dw} = w\frac{dc}{dw}$$

$$\frac{d^2c}{dr^2} = \frac{d}{dw}\left[\sqrt{\frac{K_v}{D}}\frac{dc}{dw}\right]\frac{dw}{dr} = \sqrt{\frac{K_v}{D}}\sqrt{\frac{K_v}{D}}\frac{d^2c}{dw^2} = \frac{K_v}{D}\frac{d^2c}{dw^2}$$

$$r^2\frac{d^2c}{dr^2} = \frac{1}{\frac{K_v}{D}} W^2\frac{K_v}{D}\frac{d^2c}{dw^2} = W^2\frac{d^2c}{dw^2}$$

The differential equation in terms of W becomes:

$$W^2\frac{d^2c}{dw^2} + W\frac{dc}{dw} - W^2C = 0$$

The second order ordinary differential equation is a Modified Bessel Function, which can be solved using a series solution in terms of W:

$$\text{Let} \quad C(W) = \sum_{t=0}^{\infty} a_t W^t$$

$$C'(W) = \sum_{t=0}^{\infty} a_t \cdot tW^{t-1}$$

$$C''(W) = \sum_{t=0}^{\infty} a_t \cdot t(t-1) W^{t-2}$$

$$W^2C'' + WC' - W^2C = 0$$

The series form of the differential equation is:

$$\sum_{t=0}^{\infty} a_t \cdot t(t-1) W^t + \sum_{t=0}^{\infty} a_t \cdot tW^t - \sum_{t=0}^{\infty} a_t W^{t+2} = 0$$

$$\sum_{t=2}^{\infty} a_t \, t(t-1) W^t + \sum_{t=1}^{\infty} a_t \cdot tW^t - \sum_{t=0}^{\infty} a_t W^{t+2} = 0$$

This equation is used to solve for the $a_1$ term:

$$a_1 W + \sum_{t=2}^{\infty} a_t \cdot t(t-1) W^t + \sum_{t=2}^{\infty} a_t tW^t - \sum_{t=0}^{\infty} a_t W^{t+2} = 0$$

$$j = t - 2 \qquad\qquad j = t - 2$$

At this point, changing the index is used to match powers with the last term:

$\Rightarrow$ $a_1 = 0$ since the w-terms are linearly independent:

$$\sum_{j=0}^{\infty} a_{j+2} \, (j+2)(j+1) \, W^{j+2} + \sum_{j=0}^{\infty} a_{j+2} \, (j+2) \, W^{j+2}$$

$$-\sum_{j=0}^{\infty} a_j W^{j+2} = 0$$

The equation can be simplified into:

$$\sum_{j=0}^{\infty} \{a_{j+2}[(j+2)(j+1) + (j+2)] - aj\} W^{j+2} = 0$$

The coefficients must be zero since the $W^{j+2}$ are linearly independent.

For the even values:

$$a_{j+2}(j+2)[(j+1)+1] = aj$$

$$a_{j+2} = \frac{aj}{(j+2)^2} \qquad \text{recall } a_1 = 0$$

$$\begin{aligned}
a_2 &= \frac{a_0}{2^2} \\
a_4 &= \frac{a_2}{4^2} \\
&= \frac{a_0}{4^2 \cdot 2^2} \\
a_6 &= \frac{a_4}{6^2} \\
&= \frac{a_0}{6^2 \cdot 4^2 \cdot 2^2} \\
a_8 &= \frac{a_0}{8^2 \cdot 4^2 \cdot 2^2} \\
&\vdots \qquad\qquad \vdots \\
a_{2j} &= \frac{a_0}{\prod_{t=1}^{j} (2t)^2}
\end{aligned}$$

For the odd values, all odd coefficients are zero, since they are linearly dependent on the

$a_1$ coefficient.

$$a_3 = \frac{a_1}{3^2} = 0$$

$$a_5 = \frac{a_3}{5^2} = 0$$

$$\vdots \qquad \vdots$$

$$a_{2j+1} = 0$$

The even coefficients can be rewritten as a product under the summation:

$$a_6 = \frac{a_0}{\prod_{t=1}^{3} (2t)^2}$$

$$= \frac{a_0}{2^2 \cdot 4^2 \cdot 6^2}, \text{ as before}$$

$$C(W) = a_0 \sum_{t=0}^{\infty} \frac{1}{\prod_{K=1}^{t} (2K)^2} W^{2t}$$

$$\text{where } \prod_{K=1}^{0} (2K)^2 =: 1$$

By our own definition:

$$W =: \varphi \frac{r}{R}$$

$$C(r) = a_0 \sum_{t=0}^{\infty} \frac{1}{\prod_{K=1}^{t} (2K)^2} \varphi^{2t} \left(\frac{r}{R}\right)^{2t}$$

At r = R:

$$C(R) = C_R = a_0 \sum_{t=0}^{\infty} \frac{\varphi^{2t}}{\prod_{K=1}^{t} (2K)^2}$$

$$a_0 = \frac{C_R}{\sum_{t=0}^{\infty} \frac{\varphi^{2t}}{\prod_{K=1}^{t} (2K)^2}}$$

$$\frac{C}{C_R} = \frac{\sum_{t=0}^{\infty} \frac{\varphi^{2t}}{\prod_{K=1}^{t} (2K)^2} \left(\frac{r}{R}\right)^{2t}}{\sum_{t=0}^{\infty} \frac{\varphi^{2t}}{\prod_{K=1}^{t} (2K)^2}}$$

which is the final solution to the first order reaction rate differential equation.

Proof that C(W) satisfies the differential equation:

$$W^2 \frac{d^2C}{dw^2} + W \frac{dC}{dw} - W^2 C = 0$$

Ignore $a_0$ since it cancels:

t = 1 term:

$$C(W) = a_0 \sum_{t=0}^{\infty} \frac{1}{\prod_{K=1}^{t} (2K)^2} W^{2t}$$

$$= a_0 \left[ 1 + \sum_{t=1}^{\infty} \frac{1}{\prod_{K=1}^{t} (2K)^2} W^{2t} \right]$$

$$\frac{dc}{dw} = \sum_{t=1}^{\infty} \frac{2t}{\prod_{K=1}^{t} (2K)^2} W^{2t-1}$$

$$\frac{d^2c}{dw^2} = \sum_{t=1}^{\infty} \frac{2t(2t-1)}{\prod_{K=1}^{t} (2K)^2} W^{2t-2}$$

$$\sum_{t=1}^{\infty} \frac{2t(2t-1) + 2t}{\prod_{K=1}^{t} (2K)^2} W^{2t} - W^2 - \sum_{t=1}^{\infty} \frac{W^{2t+2}}{\prod_{K=1}^{t} (2K)^2} = 0$$

$$\sum_{t=1}^{\infty} \frac{[(2t)^2 - W^2]}{\prod_{K=1}^{t} (2K)^2} W^{2t} - W^2 = 0$$

$\frac{4}{4} W^2 - W^2 = 0$ $\therefore$ equation is satisfied for $W^2$ term

$$\sum_{t=2}^{\infty} \frac{(2t)^2 W^{2t}}{\prod_{K=1}^{t} (2K)^2} - \sum_{t=1}^{\infty} \frac{W^{2t+2}}{\prod_{K=1}^{t} (2K)^2} = 0$$

$$2j = 2(t + 1)$$

$$j = t + 1$$

$$\sum_{t=2}^{\infty} \frac{(2t)^2 W^{2t}}{\prod_{K=1}^{t} (2K)^2} - \sum_{j=2}^{\infty} \frac{W^{2j}}{\prod_{K=1}^{j-1} (2K)^2}$$

$$\sum_{t=2}^{\infty} \left[ \frac{(2t)^2}{\prod_{K=1}^{t} (2K)^2} - \frac{1}{\prod_{K=1}^{t-1} (2K)^2} \right] W^{2t}$$

$$\sum_{t=2}^{\infty} \left[ \frac{1}{\prod_{K=1}^{t-1} (2K)^2} - \frac{1}{\prod_{K=1}^{t-1} (2K)^2} \right] W^{2t}$$

$$= 0 \text{ , as required.}$$

This proof verifies that the series solution to the differential equation satisfies both the boundary conditions for the given problem.

The equation used for the Chapman-Enskog theory requires the determination of temperature, pressure, mass of gases used, and the interaction parameters. This theory is derived from the Kinetic Theory of Gases which treats gases as spherical particles.

The equation is:

$$D = 0.0018583 \frac{\sqrt{T^3 \left( \frac{1}{M_{argon}} + \frac{1}{M_{i.r.}} \right)}}{P \sigma_{12}^2 \Omega_D}$$

# APPENDIX B

## Computer Program for Process Model

## APPENDIX B

### Computer Program for Process Model

The following BASIC listed computer program calculates the fraction of porosity in the fiber tow, the effective diffusion coefficient, and the Thiele parameter and concentration profile for the SiC system. The specific input parameters used are listed in the section on modeling.

```
5 FIRSTRUN = 0
10 CLS
30      LOCATE  8,20
40      PRINT "Diffusion/Reaction Balance Calculation"
50      LOCATE 12,31
60      PRINT "programmed by:"
70      LOCATE 17,36
80      PRINT "Mike"
90      FOR I = 1 TO 2000 : NEXT I
100     REM Main Loop
110             GOSUB 1000 : REM Get Variables
120             GOSUB 5000 : REM Main
130             GOSUB 10000: REM Restart?
1000    REM Get Variables
1030    KB      = 8.314
1040    TAU     = SQRT(2)
1050    MAR     = 40
1070    S       = 3.418
1080    WD      = 1.1
1090    D0      = .0018583
1100    CLS
1120    GOSUB 2000:REM Print Variables
1130    FOR I = 1 TO 9
1140            LOCATE 20,20:PRINT "("
```

```
1150          LOCATE 20,24:PRINT ")"
1155          LOCATE 20,21:PRINT I
1157          LOCATE 20,27:INPUT VAR
1158          IF VAR = 0  THEN 1140
1159          LOCATE 20,20: PRINT "                    "
1160          IF VAR = -1 THEN GOTO 1180
1161        IF VAR = -2 THEN GOTO 1200
1165          LOCATE 20,20: PRINT "                    "
1170          GOSUB 3000:REM Index Variables
1180          NEXT I
1190    GOTO 1130
1200    RETURN
2000    LOCATE 5,10
2010    PRINT "(1).....T  -       temperature (K) = ";T;
2015    LOCATE 6,10
2020    PRINT "(2).....P  -        pressure (atm) = ";P;
2025    LOCATE 7,10
2030    PRINT "(3).....R  -            tow radius = ";RT;
2035    LOCATE 8,10
2040    PRINT "(4).....Cs - initial concentration = ";CS;
2045    LOCATE 9,10
2050    PRINT "(5).....K0 -         rate constant = ";K0;
2055    LOCATE 10,10
2060    PRINT "(6).....Ea -    activation energy = ";EA;
2065    LOCATE 11,10
2070    PRINT "(7).....Mlr - mass of lim. reactant = ";MLR;
2075    LOCATE 12,10
2080    PRINT "(8).....r  -          fiber radius = ";RF;
2085    LOCATE 13,10
2090    PRINT "(9).....N  -        # of filaments = ";N;
2200    RETURN
3000    REM Index Variables
3010    IF I = 1 THEN T  = VAR
3020    IF I = 2 THEN P  = VAR
3030    IF I = 3 THEN RT = VAR
3050    IF I = 4 THEN CS = VAR
3060    IF I = 5 THEN K0 = VAR
3070    IF I = 6 THEN EA = VAR
3080    IF I = 7 THEN MLR= VAR
3090    IF I = 8 THEN RF = VAR
3100    IF I = 9 THEN N  = VAR
```

```
3110    GOSUB 2000
3120    RETURN
5000    REM Main
5005    GOSUB 6000 : REM Get Constants
5010 CLS
5020 LOCATE 20,20
5030 INPUT "# of points";Q
5035 IF FIRSTRUN = 0 THEN  DIM RATIO(Q)
5040 FOR I = 1 TO Q
5050    R = RT*(1-I)/(1-Q)
5065    GOSUB 9000 : REM Print Data
5070 NEXT I
5080    RETURN
6000    REM Get Constants
6005 PRINT P
6010          D     = D0*(((T^3)*((1/MAR)+(1/MLR)))^.5)/(P*(S^2)*WD)
6020          THETA = 1-(((RF/RT)^2)*N)
6030          DEFF  = D*THETA/1.414
6040          SV    = 2*RF*N/(RT^2)
6050          KS    = K0*EXP(-(EA/(KB*T)))
6060          KV    = KS*SV
6070          PHI2  = KV*(RT^2)/DEFF
6080 PROD = 1 : PHISUM = 0 : RATIO = 0
6090    RETURN
9000    REM Print Data
9010    CLS
9015    LOCATE 1,20: PRINT "Kv            =";KV
9020    LOCATE 3,20
9030    PRINT "Thiele Modulus ="; PHI2
9040    LOCATE 5,20
9050    PRINT "Deff           ="; DEFF
9055    LOCATE 7,20
9057    PRINT "Theta          = "; THETA
9060    LOCATE 10,15
9070    PRINT "   R"
9080    LOCATE 11,15
9090    PRINT "-----------"
9100    LOCATE  10,35
9110    PRINT "Cr/Cs"
9120    LOCATE  11,35
9130    PRINT "-----"
```

```
9140    FOR I = 1 TO Q
9150    LOCATE I+11, 17:RADIUS = RT*(1-I)/(1-Q)
9160    PRINT RADIUS
9170    LOCATE I+11,35
9180    PHI = PHI2^.5: W = RADIUS/RT
9181          FOR J = 0 TO 4
9182          FOR K = 1 TO J
9183            PROD = PROD * ((2*K)^2)
9184                NEXT K
9185          RATIO = RATIO + (((PHI*W)^(2*J))/PROD)
9186          PHISUM= PHISUM + ((PHI^(2*J))/PROD)
9187          NEXT J
9188          RATIO = (RATIO/PHISUM)
9189  PROD = 1
9194 PRINT RATIO : RATIO = 0 : PHISUM = 0 : PROD = 1
9195    NEXT I
9200    A$ = INKEY$
9210    IF LEN(A$) = 0 THEN 9200
9220    RETURN
10000 CLS : FIRSTRUN = 1
10010 LOCATE 20,20
10020 INPUT "Another Run(1 = YES ; 2 = No)?",ANSWER
10030 IF ANSWER = 2 THEN CLS
10040 IF ANSWER = 1 THEN GOTO 100 ELSE END
```

# APPENDIX C

## Statistical Analysis

## APPENDIX C

### Statistical Analysis

The statistical analyses were performed using the commercially available code STATGRAPHICS. This code permits determination of which process variable, or variables, have an influence on the various product attributes. Least squares regression analysis permits the fitting of equations such as the following:

$$y = A + BX_1 + CX_2 + DX_3$$

where y represents product attributes such as strength, fiber weight (or weight gain), surface roughness, and agglomeration, and $X_1$, $X_2$ and $X_3$ represent process variables such as reactor temperature, MTS flow rate, and hydrogen flow rate. For this study we also performed the analyses (using STATGRAPHICS) that permitted determination of whether the squared (e.g. $X_1^2$) and interaction terms (e.g. $X_1X_2$) should be incorporated into the model equation. For the data analyzed here, these higher order terms were generally not statistically significant so the above equation containing only linear terms was used. It can be seen from Table C-1 that the equation relating fiber weight (mg) after coating to the process variables ($X_1$ = temperature, $X_2$ = MTS flow rate, and $X_3$ = hydrogen flow rate) is:

$$\text{Fiber Weight} = -0.106858 + (1.33727E\text{-}4)\,X_1 + (6.7476E\text{-}3)\,X_2 - (0.0128031)\,X_3$$

Once the constants for the above regression equation are determined it is possible, again using STATGRAPHICS, to generate contour plots such as the ones shown in Figures 25 and 26. These plots are generated from the regression equation and are the best predictions of how the process variables influence the particular response variable (product attribute) being studied.

Another useful statistical procedure is generation of the analysis of variance table (see Tables C-1 to C-3). This analysis shows how much of the variation of the response is caused by the process variables. For example, the "Sum of Squares" column in Table C-1 shows that the MTS flow rate (sum of squares = 0.004997) accounts for more of the variation observed for fiber weight than the other two process variables. The same column shows that temperature had a stronger influence than hydrogen flow rate. The column labeled "Mean Square" is obtained by dividing the sum of squares by the degrees of freedom. The column labeled "F-Ratio" is obtained by dividing the mean square by the "error mean square". The F-Ratio is useful in that it permits quantification of the confidence we have that a particular process variable is having a real influence on the response. For example, the right most column, labeled "P-Value", is the probability that data showing this much variation (or correlation with a particular process variable) would have been obtained even if there was not a real cause and effect relationship. For example, in Table C-1 the "P-Value" for "Temperature" is 0.0040. This means that if temperature was not influencing the fiber weight (i.e. the amount of coating deposited) then data showing this much correlation between fiber weight and temperature would be obtained (on average) only 4 times out of 1000 trials. That is, we are 99.6% confident that the reactor temperature influences the fiber weight.

Other useful values are included in the following tables. The first column of numbers gives the values for the coefficients (e.g. A, B, C, and D) in the model equation. The correlation coefficient ($R^2$) is a measure of how well the regression equation describes the experimental data, i.e., a measure of the degree of fit. The $R^2$ value theoretically varies from zero to unity. Values closer to unity indicate a better fit.

Table C-1. Analysis of Variance for Fiber Weight (mg).

| Effect | Regression Coefficient | Sum of Squares | D.F. | Mean Square | F-Ratio | P-Value |
|---|---|---|---|---|---|---|
| Constant (i.e., A) | -0.106858 | | | | | |
| Temperature (°C) | 1.33727E-4 | 0.00294869 | 1 | 0.0029487 | 12.63 | 0.0040 |
| MTS Flow Rate (g/min) | 6.7476E-3 | 0.00499673 | 1 | 0.0049967 | 21.41 | 0.0006 |
| Hydrogen Flow Rate (ℓ/min) | -0.0128031 | 0.00096938 | 1 | 0.0009694 | 4.15 | 0.0642 |
| Error | | 0.00280111 | 12 | 0.0002334 | | |
| Total | | 0.01311668 | 15 | | | |

R-squared = 0.786

Table C-2. Analysis of Variance for Surface Roughness (arbitrary scale from 1 to 10 with 10 being roughest).

| Effect | Regression Coefficient | Sum of Squares | D.F. | Mean Square | F-Ratio | P-Value |
|---|---|---|---|---|---|---|
| Constant (i.e., A) | -4.52767 | | | | | |
| Temperature (°C) | 9.12269E-3 | 13.7226148 | 1 | 13.7226148 | 3.38 | 0.0907 |
| MTS Flow Rate (g/min) | 0.341039 | 12.7642586 | 1 | 12.7642586 | 3.15 | 0.1014 |
| Hydrogen Flow Rate ($\ell$/min) | -2.33477 | 32.2368567 | 1 | 32.236857 | 7.95 | 0.0155 |
| Error | | 48.6660916 | 12 | 4.055508 | | |
| Total | | 113.000000 | 15 | | | |

R-squared = 0.569

Table C-3. Analysis of Variance for Agglomeration (%).

| Effect | Regression Coefficient | Sum of Squares | D.F. | Mean Square | F-Ratio | P-Value |
|---|---|---|---|---|---|---|
| Constant (i.e., A) | -139.323 | | | | | |
| Temperature (°C) | 0.138539 | 3164.7003 | 1 | 3164.700 | 5.69 | 0.0344 |
| MTS Flow Rate (g/min) | 9.57144 | 10054.0619 | 1 | 10054.0619 | 18.08 | 0.0011 |
| Hydrogen Flow Rate (ℓ/min) | -13.3184 | 1048.9897 | 1 | 1048.9897 | 1.89 | 0.1948 |
| Error | | 6674.2691 | 12 | 556.189 | | |
| Total | | 22946.4375 | 15 | | | |

R-squared = 0.709



U.S. GOVERNMENT PRINTING OFFICE 750-113